EUROPEAN ORGANIZATION FOR NUCLEAR RESEARCH (CERN)

CERN-EP-2021-117
2021/07/03

CMS-TOP-18-010

# Measurement of the inclusive and differential $\mathrm{t\bar{t}}\gamma$ cross sections in the single-lepton channel and EFT interpretation at $\sqrt{s} = 13\,\mathrm{TeV}$

The CMS Collaboration[*]

## Abstract

The production cross section of a top quark pair in association with a photon is measured in proton-proton collisions at a center-of-mass energy of 13 TeV. The data set, corresponding to an integrated luminosity of $137\,\mathrm{fb}^{-1}$, was recorded by the CMS experiment during the 2016–2018 data taking of the LHC. The measurements are performed in a fiducial volume defined at the particle level. Events with an isolated, highly energetic lepton, at least three jets from the hadronization of quarks, among which at least one is b tagged, and one isolated photon are selected. The inclusive fiducial $\mathrm{t\bar{t}}\gamma$ cross section, for a photon with transverse momentum greater than 20 GeV and pseudorapidity $|\eta| < 1.4442$, is measured to be $800 \pm 7\,(\mathrm{stat}) \pm 46\,(\mathrm{syst})\,\mathrm{fb}$, in good agreement with the prediction from the standard model at next-to-leading order in quantum chromodynamics. The differential cross sections are also measured as a function of several kinematic observables and interpreted in the framework of the standard model effective field theory (EFT), leading to the most stringent direct limits to date on anomalous electromagnetic dipole moment interactions of the top quark and the photon.

*Submitted to the Journal of High Energy Physics*

---

[*] See Appendix A for the list of collaboration members

# 1 Introduction

The large amount of proton-proton (pp) collision data at a center-of-mass energy of 13 TeV at the LHC allows for precision measurements of standard model (SM) processes with small production rates. Among these, top quark production provides a testing ground for the SM predictions and for phenomena beyond the SM (BSM). In particular, measurements of the inclusive and differential cross sections of top quark pair production in association with a high-energy photon ($\mathrm{t\bar{t}}\gamma$) allow us to constrain anomalous $\mathrm{t\bar{t}}\gamma$ electroweak interactions [1–4].

The CDF Collaboration at the Fermilab Tevatron measured the $\mathrm{t\bar{t}}\gamma$ production cross section using proton-antiproton collisions at $\sqrt{s} = 1.96\,\mathrm{TeV}$ [5], while at the LHC the measurement was performed in pp collisions at 7 TeV by the ATLAS [6], and at 8 TeV by both the ATLAS [7] and CMS [8] Collaborations. At 13 TeV, the ATLAS Collaboration measured the $\mathrm{t\bar{t}}\gamma$ production cross section in leptonic [9] and in the $\mathrm{e}\mu$ [10] final states. All of these results are in agreement with the SM.

In this paper, the inclusive and differential $\mathrm{t\bar{t}}\gamma$ production cross sections are measured in pp collisions at $\sqrt{s} = 13\,\mathrm{TeV}$. The analysis uses a data sample recorded with the CMS detector during Run 2 (2016–2018) of the LHC, which corresponds to an integrated luminosity of $137\,\mathrm{fb}^{-1}$. The measurement is performed in the single-lepton (electron or muon) final state in a fiducial region defined at particle level. The inclusive fiducial $\mathrm{t\bar{t}}\gamma$ cross section is measured for a selection on the photon transverse momentum of $p_{\mathrm{T}}(\gamma) > 20\,\mathrm{GeV}$ and the pseudorapidity of $|\eta(\gamma)| < 1.4442$, corresponding to the barrel region of the CMS electromagnetic calorimeter (ECAL). Differential cross sections are measured in the same fiducial region as a function of $p_{\mathrm{T}}(\gamma)$, $|\eta(\gamma)|$, and the angular separation between the lepton and the photon, $\Delta R(\ell,\gamma)$. The observations are interpreted in the context of the SM effective field theory (SM-EFT) [11], where the $c_{\mathrm{tZ}}$ and $c_{\mathrm{tZ}}^{\mathrm{I}}$ operators, defined in Ref. [12], are constrained using the measurement of the distribution of $p_{\mathrm{T}}(\gamma)$. Tabulated results are provided in HEPDATA [13]. Examples of Feynman diagrams at leading order (LO) contributing to the $\mathrm{t\bar{t}}\gamma$ signal topology are shown in Fig. 1.

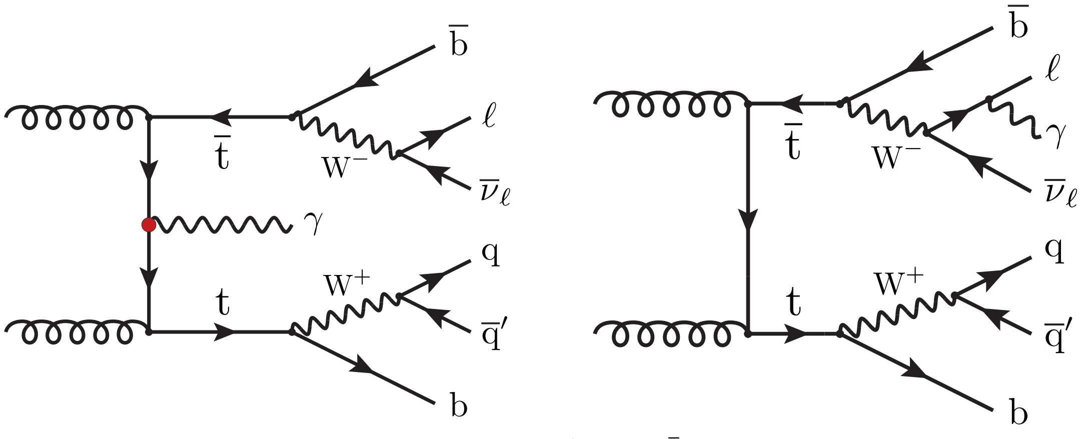

Figure 1: Representative LO Feynman diagrams for the $\mathrm{t\bar{t}}\gamma$ signal process in the single-lepton channel, where the highly energetic photon originates from the top quark (left), or is emitted from a lepton (right). The $\mathrm{t\bar{t}}\gamma$ interaction vertex is indicated by a circle.

This paper is organized as follows. The CMS detector is briefly introduced in Section 2. Details on the simulation of the signal and background processes and their modeling are provided in Section 3. The online selection, event reconstruction, and object definitions are described in Section 4. The fiducial phase space definition and photon categorization are described in Section 5. The event selection and the statistical treatment are discussed in Section 6. The procedures to estimate the backgrounds are described in Section 7 and the systematic uncertainties are discussed in Section 8. The obtained results and the interpretation of the measurements in the context of SM-EFT are presented in Section 9. Finally, a summary is provided in Section 10.

## 2 The CMS detector

The central feature of the CMS apparatus is a superconducting solenoid of 6 m internal diameter, providing a magnetic field of 3.8 T. Within the solenoid volume are a silicon pixel and strip tracker, a lead tungsten crystal ECAL, and a brass and scintillator hadron calorimeter (HCAL), each composed of a barrel and two endcap sections. Forward calorimeters extend the $\eta$ coverage provided by the barrel and endcap detectors that improve the measurement of the imbalance in transverse momentum. Muons are detected in gas-ionization chambers embedded in the steel flux-return yoke outside the solenoid.

Events of interest are selected using a two-tiered trigger system [14]. The first level trigger (L1) [15], composed of custom hardware processors, uses information from the calorimeters and muon detectors to select events at a rate of around 100 kHz within a fixed latency of about 4 $\mu$s. The second level, known as the high-level trigger, consists of a farm of processors running a version of the full event reconstruction software optimized for fast processing, and reduces the event rate to around 1 kHz before data storage [14]. A more detailed description of the CMS detector, together with a definition of the coordinate system used and the relevant kinematic variables, can be found in Ref. [16].

## 3 Simulated event samples

Multiple Monte Carlo (MC) event generators are used to simulate the background and signal contributions, matching the varying conditions for each data-taking period. The $\mathrm{t\bar{t}}$, $t$-channel single top quark, tW, and WW background processes are simulated at next-to-LO (NLO) in perturbative quantum chromodynamics (QCD) with the POWHEG v2 [17–23] event generator. The QCD multijet processes are generated with PYTHIA v8.226 (8.230) [24] for the 2016 (2017, 2018) data-taking period. All other background processes are simulated with MADGRAPH5_aMC@NLO v2.6.0 [25] at LO or NLO accuracy. The $\mathrm{t\bar{t}}$ simulation is normalized to a cross section of $832 \pm 42$ pb calculated with the TOP++ v2.0 program [26] at next-to-NLO (NNLO), including resummation of next-to-next-to-leading-logarithm (NNLL) soft-gluon terms [27–32]. Events with an $s$- or $t$-channel produced top quark are normalized to NLO cross sections [33, 34], while the normalizations of WW and tW are at NNLO [35]. Drell–Yan and W+jets events are generated with up to four extra partons in the matrix element calculations with MADGRAPH5_aMC@NLO at LO and are normalized to NNLO cross sections [36–38] including electroweak corrections at NLO [39, 40]. The $\mathrm{t\bar{t}Z}$, $\mathrm{t\bar{t}W}$, tZq, $\mathrm{t}\gamma$, $\mathrm{W}\gamma$, $\mathrm{Z}\gamma$, and other diboson processes (VV, with V either W or Z) are normalized to the most precise cross sections available [41, 42].

The $\mathrm{t\bar{t}}\gamma$ signal is generated with MADGRAPH5_aMC@NLO at LO as a doubly resonant $2 \to 7$ process including all decay channels of the intermediate W bosons. It includes events where the photon is radiated from the intermediate top quarks, the intermediate W bosons and their decay products, the b quarks, and, in the case of quark-antiquark annihilation, radiation from initial-state quarks. The photon is required to satisfy $p_{\mathrm{T}} > 10\,\mathrm{GeV}$ and $|\eta| < 5$, while the lepton must pass $|\eta| < 5$. The angular separation $\Delta R$ between the photon and any of the seven final-state particles is required to be greater than 0.1, where $\Delta R = \sqrt{(\Delta\eta)^2 + (\Delta\phi)^2}$ and $\phi$ denotes the azimuthal angle. The renormalization scale ($\mu_{\mathrm{R}}$) and factorization scale ($\mu_{\mathrm{F}}$) are set to $\frac{1}{2}\sum_i \sqrt{{m_i}^2 + {p_{\mathrm{T},i}}^2}$, where the sum runs over all final-state particles generated at the matrix-element (ME) level. Although no photons are simulated at the ME level in the $\mathrm{t\bar{t}}$ process, initial- and final-state photon radiation is accounted for in the showering algorithm. We remove double counting of the $\mathrm{t\bar{t}}$ and $\mathrm{t\bar{t}}\gamma$ samples by excluding events from the $\mathrm{t\bar{t}}$ sample with a generated photon passing the photon requirements of the $\mathrm{t\bar{t}}\gamma$ signal sample. The overlap between W$\gamma$ and W+jets, Z$\gamma$ and Drell–Yan, and t$\gamma$ and the single top quark *t*-channel process is removed analogously.

Table 1: Event generator, perturbative order in QCD of the simulation, and perturbative order of the cross section normalization for each process.

| Process | Event generator | Perturbative order of simulation | Cross section normalization |
|---|---|---|---|
| $\mathrm{t\bar{t}}\gamma$ | MADGRAPH5_aMC@NLO | LO | NLO |
| $\mathrm{t\bar{t}}$ | POWHEG | NLO | NNLO+NNLL [26–32] |
| Single t (*t*-channel) | POWHEG | NLO | NLO [33, 34] |
| Single t (*s*-channel) | MADGRAPH5_aMC@NLO | NLO | NLO [33, 34] |
| tW | POWHEG | NLO | NNLO [35] |
| Drell–Yan, W+jets | MADGRAPH5_aMC@NLO | LO | NNLO [36–40] |
| W$\gamma$ | MADGRAPH5_aMC@NLO | LO | NLO |
| WW | POWHEG | NLO | NNLO [43] |
| t$\gamma$, Z$\gamma$, WZ, ZZ<br>$\mathrm{t\bar{t}}$Z, $\mathrm{t\bar{t}}$W, tZq | MADGRAPH5_aMC@NLO | NLO | NLO |
| Multijet | PYTHIA | LO | LO |

The event generators are interfaced with PYTHIA v8.226 (8.230) using the CP5 tune [44–46] for the 2016 (2017, 2018) samples to simulate multiparton interactions, fragmentation, parton shower, and hadronization of partons in the initial and final states, along with the underlying event. The NNPDF parton distribution functions (PDFs) v3.1 [47] are used according to the different perturbative order in QCD at the ME level. For the 2016 data-taking period, the CUETP8M1 tune [45] and the NNPDF PDFs v3.0 [48] are used for the Drell–Yan, W+jets, t$\gamma$, Z$\gamma$, W$\gamma$, diboson, $\mathrm{t\bar{t}}$W, $\mathrm{t\bar{t}}$Z, tZq, and multijet processes. Double counting of the partons generated with MADGRAPH5_aMC@NLO and PYTHIA is removed using the MLM [49] and the FXFX [50] matching schemes for LO and NLO samples, respectively. The events are subsequently processed with a GEANT4-based simulation model [51] of the CMS detector. All simulated samples include the effects of additional pp collisions in the same or adjacent bunch crossings (pileup), and are reweighted according to the observed distribution of the number of interactions in each bunch crossing [52]. In the following, to simplify the notation, the single top quark, $\mathrm{t\bar{t}}$, and t$\gamma$ processes are grouped in the t/$\mathrm{t\bar{t}}$ category, and furthermore, the tZq, $\mathrm{t\bar{t}}$W, $\mathrm{t\bar{t}}$Z, WW, WZ, and ZZ processes in a category labeled "other". A summary of the event samples is provided in Table 1.

## 4 Event reconstruction

Events are selected at the high-level trigger by the algorithms that require the presence of at least one lepton ($\ell = \mathrm{e}$ or $\mu$). The trigger threshold on the leading muon $p_{\mathrm{T}}$ is 27 (24) GeV in the 2017 (2016 and 2018) LHC running period. For electrons, the trigger threshold in the 2016 (2017–2018) period is 27 (32) GeV.

The particle-flow (PF) algorithm [53] aims to reconstruct and identify each individual particle in an event, with an optimized combination of information from the various elements of the CMS detector. The candidate vertex with the largest value of summed physics-object $p_{\mathrm{T}}^2$ is taken to be the primary pp interaction vertex (PV). The energy of charged PF hadrons is determined from a combination of the track momentum and the matching ECAL and HCAL energy deposits, corrected for zero-suppression effects and for the response function of the calorimeters to hadronic showers. The energy of neutral PF hadrons is obtained from the corresponding corrected ECAL and HCAL energies.

The energy of electrons is determined from a combination of the electron momentum at the PV as determined by the tracker, the energy of the corresponding ECAL cluster, and the energy sum of all bremsstrahlung photons spatially compatible with originating from the electron track. Electron candidates are required to satisfy $p_{\mathrm{T}} > 35\,\mathrm{GeV}$ and $|\eta| < 2.4$, excluding the transition region between the barrel and endcap of the ECAL, $1.4442 < |\eta| < 1.5660$. The electron identification is performed using shower shape variables, track-cluster matching variables, and track quality variables. To reject electrons originating from photon conversion inside the detector, electrons are required to miss at most one possible hit in the innermost tracker layer and to be incompatible with any conversion-like secondary vertices.

The momentum of muons is obtained from the curvature of the corresponding track. Muon candidates are selected having $p_{\mathrm{T}} > 30\,\mathrm{GeV}$ and $|\eta| < 2.4$. The identification of muon candidates is performed using the quality of the geometrical matching between the measurements of the tracker and muon system [54].

The energy of photons is obtained from the ECAL measurement. Photon candidates are required to satisfy $p_{\mathrm{T}}(\gamma) > 20\,\mathrm{GeV}$ and to fall within the barrel of the ECAL, $|\eta| < 1.4442$. The identification of photons is based on isolation and shower shape information as a function of $p_{\mathrm{T}}$ and $\eta$, and takes into account pileup effects [55, 56]. In particular, the lateral shower extension must satisfy $\sigma_{\eta\eta}(\gamma) < 0.01$ for the chosen "medium" photon working point [57].

All lepton and photon candidates are required to be isolated from other objects by selecting the reconstructed charged and neutral PF candidates in a cone around the candidate. A radius $\Delta R = 0.3$ (0.4) is used for electron (muon) candidates. For electron candidates, $p_{\mathrm{T}}$- and $\eta$-dependent thresholds are set on the pileup corrected scalar $p_{\mathrm{T}}$ sum of photons and neutral and charged hadrons reconstructed by the PF algorithm ($I_{\mathrm{rel}}(\mathrm{e})$) in the range of 5–10%. The chosen "tight" electron working point has a 70% efficiency while rejecting electron candidates originating from jets [57]. A muon candidate is isolated if it satisfies $I_{\mathrm{rel}}(\mu) < 0.15$. The efficiency of the chosen "tight" working point is 90–95%, depending on $p_{\mathrm{T}}$ and $\eta$ of the muon candidate [54]. For photon candidates, the scalar $p_{\mathrm{T}}$ sum of the charged particles within a cone of $\Delta R = 0.3$, denoted as the photon charged-hadron isolation, must satisfy $I_{\mathrm{chg}}(\gamma) \leq 1.141\,\mathrm{GeV}$. Depending on the photon candidate $p_{\mathrm{T}}$, there are separate requirements on the photon neutral-hadron and total isolation [57]. The photon reconstruction and selection efficiency for the chosen "medium" working point in simulation is on average 80%. It is corrected as a function of the $p_{\mathrm{T}}$ and $\eta$ of the reconstructed photon to match the efficiency observed in data.

Furthermore, "loose" selection criteria are used to define control regions and for the purpose to veto events with additional reconstructed leptons. With respect to the tight electron selection, the transverse momentum requirement is relaxed to $p_{\mathrm{T}} > 15\,\mathrm{GeV}$, the threshold on $I_{\mathrm{rel}}(\mathrm{e})$ to the range of 20–25%, depending on $p_{\mathrm{T}}$ and $\eta$ of the electron candidate, and two (three) missed hits in the innermost tracker layers are allowed for electrons in the barrel (endcap) region. The loose muon selection is based on Ref. [58] with $p_{\mathrm{T}} > 15\,\mathrm{GeV}$ and $I_{\mathrm{rel}}(\mu) < 0.25$ [58]. The loose photon selection has a relaxed $I_{\mathrm{chg}}(\gamma)$ requirement of $I_{\mathrm{chg}}(\gamma) \leq 1.694\,\mathrm{GeV}$ and a 90% identification efficiency for photons within the barrel section of the ECAL [57].

Jets are reconstructed by clustering PF candidates using the anti-$k_\mathrm{T}$ algorithm [59, 60] with a distance parameter of 0.4. Selected jets are required to satisfy $p_\mathrm{T} > 30\,\mathrm{GeV}$ and $|\eta| < 2.4$. Contributions to the clustered energy from pileup interactions are corrected for by requiring charged-hadron candidates to be associated with the PV and an offset correction for the contribution from neutral hadrons falling within the jet area is subtracted from the jet energy. Corrections to the jet energy scale (JES) are applied in simulation and data. The jet energy resolution (JER) is corrected in simulation to match the resolution observed in data [61].

Jets originating from the hadronization of b quarks are identified (b tagged) with a deep neural network algorithm [62] based on tracking and secondary vertex information. A working point is chosen such that the efficiency to identify the b jet is 55–70% for a jet $p_\mathrm{T}$ of 20–400 GeV. The misidentification rate in this $p_\mathrm{T}$ range is 1–2% for light-flavor and gluon jets, and up to 12% for charm quark jets. A correction is applied to the simulation to match the b tagging efficiencies observed in data.

The missing transverse momentum vector, $\vec{p}_\mathrm{T}^\mathrm{miss}$, is defined as the projection onto the plane perpendicular to the beams of the negative vector momentum sum of all PF candidates in an event. The JES and JER corrections are included in the $\vec{p}_\mathrm{T}^\mathrm{miss}$ computation. Its magnitude is referred to as $p_\mathrm{T}^\mathrm{miss}$.

# 5 Fiducial phase space definition and photon classification

The fiducial region of the analysis is defined at the particle level by applying an event selection to the stable particles after the event generation, parton showering, and hadronization, but before the detector simulation.

Electrons (muons) must have $p_\mathrm{T} > 35$ (30) GeV and $|\eta| < 2.4$, and must not originate from hadron decays. To account for final-state photon radiation, the four-momenta of photons inside a cone of $\Delta R = 0.1$ are added to the lepton before the lepton selection [63]. Events with leptonically decaying $\tau$ leptons in the decay chain of the top quark are considered signal.

Photons are selected if they do not originate from hadron decays, satisfy $p_\mathrm{T}(\gamma) > 20\,\mathrm{GeV}$ and $|\eta(\gamma)| < 1.4442$, and are found outside a cone of $\Delta R = 0.4$ around the leptons. An isolation requirement is applied by removing photons with stable particles (except neutrinos) found within a cone of $\Delta R = 0.1$ that satisfy $p_\mathrm{T} > 5\,\mathrm{GeV}$.

Particle-level jets are clustered using the anti-$k_\mathrm{T}$ algorithm with a distance parameter of 0.4, using all final-state particles, excluding neutrinos. Jets must satisfy $p_\mathrm{T} > 30\,\mathrm{GeV}$ and $|\eta| < 2.4$. A ghost matching method [64] is used to determine the flavor of the jets, with those matched to b hadrons tagged as b jets. Finally, the overlap of jets and other candidates is removed by excluding jets with $\Delta R \leq 0.4$ $(0.1)$ to lepton (photon) candidates. A summary of the object definitions at particle level is provided in Table 2.

The fiducial region is constructed by requiring exactly one photon, exactly one lepton, and three or more jets among which at least one must be b tagged. The inclusive fiducial cross section, predicted with MADGRAPH5_aMC@NLO at NLO in QCD, is 773 ± 135 fb.

To facilitate the estimation of backgrounds with nonprompt and misidentified photons, a photon categorization is based on the matching between the reconstructed photon and simulated particles. Reconstructed photons are matched in $\Delta R$ to the corresponding generator-level particle from the primary interaction. The maximum $\Delta R$ considered for matching is 0.3 and the $p_\mathrm{T}(\gamma)$ is required to be within 50% of the matched particle. Simulated events with a recon-

Table 2: Overview of the definition of fiducial regions for various objects at particle level. A photon is isolated, if there are no stable particles (except neutrinos) with $p_{\mathrm{T}} > 5\,\mathrm{GeV}$ within a cone of $\Delta R = 0.1$.

| Photon | e ($\mu$) | Jet | b jet |
|---|---|---|---|
| $p_{\mathrm{T}} > 20\,\mathrm{GeV}$ | $p_{\mathrm{T}} > 35$ (30) GeV | $p_{\mathrm{T}} > 30\,\mathrm{GeV}$ | $p_{\mathrm{T}} > 30\,\mathrm{GeV}$ |
| $\lvert\eta\rvert < 1.4442$ | $\lvert\eta\rvert < 2.4$ | $\lvert\eta\rvert < 2.4$ | $\lvert\eta\rvert < 2.4$ |
| no hadronic origin | no hadronic origin | $\Delta R(\text{jet}, \ell) > 0.4$ | $\Delta R(\text{b jet}, \ell) > 0.4$ |
| $\Delta R(\ell, \gamma) > 0.4$ | | $\Delta R(\text{jet}, \gamma) > 0.1$ | $\Delta R(\text{b jet}, \gamma) > 0.1$ |
| isolated | | | matched to b hadrons |

structed photon are subsequently classified into three categories based on the matched generator particle. In the “genuine photon” category, the reconstructed photon is matched to a generated photon that originates from a lepton, a W boson, or a quark. In the “misidentified electron” category, the photon is matched to an electron. The “nonprompt photon” category is comprised of events where the photon is matched to a generated photon that originates from a hadron (71%), or in absence of a match to a generated photon or electron. This category thus includes contributions with misidentified photons and photons that originate from pileup interactions (29%).

# 6 Analysis strategy

## 6.1 Signal and control region definitions

The $\mathrm{t\bar{t}}\gamma$ process typically produces events with large jet and b-tagged jet multiplicities, and an isolated photon with large $p_{\mathrm{T}}$. The measurement is performed in signal regions with exactly one lepton ($N_{\ell} = 1$), exactly one photon ($N_{\gamma} = 1$), and at least three jets ($N_{\mathrm{j}} \geq 3$), among which at least one is b tagged ($N_{\mathrm{b}} \geq 1$). Events with additional leptons or photons passing the loose selection are removed. The measurement is performed in the $N_{\mathrm{j}} = 3$ and $\geq$4 signal selections, denoted by SR3 and SR4p, respectively. The $N_{\mathrm{j}} \geq 3$ selection is denoted by SR3p. Figure 2 shows some kinematic distributions in the SR3p region where the simulated event samples are categorized according to the origin of the photon. In this figure, $M_3$ denotes the invariant mass of the three-jet combination among all identified jets that maximizes the magnitude of the vector $p_{\mathrm{T}}$ sum [65]. This choice preferentially captures the hadronic top quark decay products.

The dominant background sources are estimated from data, where simulation predicts a significant background contribution from nonprompt photons (23%), misidentified electrons (19%), and a small contribution from multijet events in the SR3p region. The nonprompt photon contribution is estimated using background-enriched control regions with relaxed criteria on $I_{\mathrm{chg}}(\gamma)$ and $\sigma_{\eta\eta}(\gamma)$. The multijet contributions to the signal and control regions are estimated by rescaling suitable normalized distributions (templates) obtained from background-enriched high-$I_{\mathrm{rel}}(\ell)$ sidebands. The misidentified electron background is estimated in a $N_{\mathrm{b}} = 0$ region where the invariant mass of the electron and photon candidates are consistent with the Z boson hypothesis [66] within 10 GeV, i.e., $\lvert m(\mathrm{e}, \gamma) - m_{\mathrm{Z}}\rvert \leq 10\,\mathrm{GeV}$, where $m_{\mathrm{Z}}$ is the Z boson mass. The control region is denoted by misDY3 (misDY4p) for $N_{\mathrm{j}} = 3$ ($\geq$4). The $\mathrm{W}\gamma$ and the $\mathrm{Z}\gamma$ processes contribute events with genuine photons to both the signal regions and the misDY3 and misDY4p control regions. In the electron channel, their contribution is constrained in “low mass” (LM) and “high mass” (HM) regions, defined by $m(\mathrm{e}, \gamma) < m_{\mathrm{Z}} - 10\,\mathrm{GeV}$ and $m(\mathrm{e}, \gamma) > m_{\mathrm{Z}} + 10\,\mathrm{GeV}$, respectively. In the muon channel, the LM (HM) region is defined by

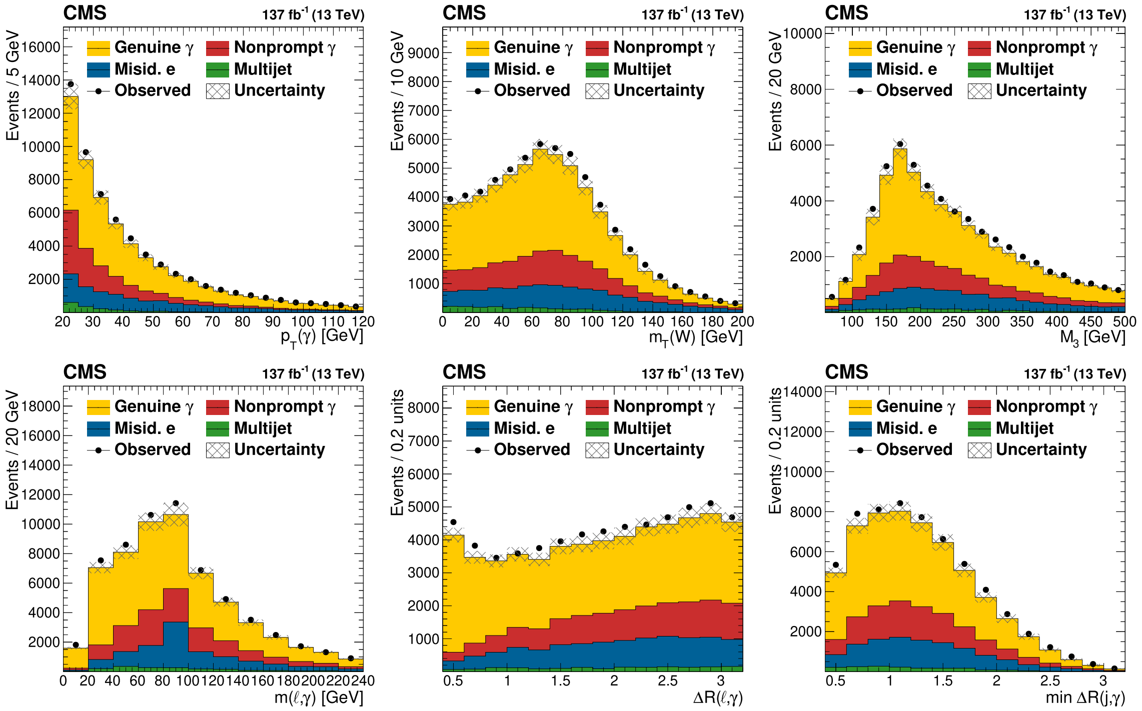

Figure 2: Distribution of $p_T(\gamma)$, the transverse mass $m_T(W)$ of the W boson candidate, the three-jet invariant mass $M_3$ (upper row); the invariant mass $m(\ell,\gamma)$ of the lepton and the photon, the angular separation $\Delta R(\ell,\gamma)$ of the lepton and the photon, and the minimal angular separation $\min \Delta R(j,\gamma)$ of the photon and all jets (lower row) in the SR3p region. The backgrounds are normalized according to the methods described in Sec. 7. The systematic uncertainties are shown as a hatched band.

Table 3: Overview of signal and control regions.

| Region | | $N_\ell$ | $N_j$ | $N_b$ | $N_\gamma$ | Other requirements |
|---|---|---|---|---|---|---|
| SR3p | SR3 | 1 | 3 | $\geq 1$ | 1 | |
| | SR4p | 1 | $\geq 4$ | $\geq 1$ | 1 | |
| LM3p | LM3 | 1 | 3 | 0 | 1 | $m(e,\gamma) < m_Z - 10\,\text{GeV}$,<br>$m(\mu,\gamma) < m_Z$ |
| | LM4p | 1 | $\geq 4$ | 0 | 1 | $m(e,\gamma) < m_Z - 10\,\text{GeV}$,<br>$m(\mu,\gamma) < m_Z$ |
| HM3p | HM3 | 1 | 3 | 0 | 1 | $m(e,\gamma) > m_Z + 10\,\text{GeV}$,<br>$m(\mu,\gamma) > m_Z$ |
| | HM4p | 1 | $\geq 4$ | 0 | 1 | $m(e,\gamma) > m_Z + 10\,\text{GeV}$,<br>$m(\mu,\gamma) > m_Z$ |
| misDY3p | misDY3 | 1 | 3 | 0 | 1 | $\lvert m(e,\gamma) - m_Z \rvert \leq 10\,\text{GeV}$ |
| | misDY4p | 1 | $\geq 4$ | 0 | 1 | $\lvert m(e,\gamma) - m_Z \rvert \leq 10\,\text{GeV}$ |

$m(\mu,\gamma) < m_Z$ ($m(\mu,\gamma) > m_Z$). Table 3 provides a summary of the kinematic requirements in the signal and control regions.

### 6.2 Statistical treatment

The signal cross section is extracted from signal and control regions using the statistical procedure detailed in Refs. [67, 68]. The observed yields, signal and background estimates in each analysis category, and the systematic uncertainties are used to construct a binned likelihood function $L(r, \theta)$ as the product of Poisson probabilities of all bins. The nuisances related to the systematic uncertainties in the experiment and in the modelling of signal and background processes are described by log-normal probability density functions. The parameter $r$ is the signal strength modifier, i.e., the ratio between the measured cross section and the cross section predicted by simulation, and $\theta$ represents the set of nuisance parameters describing the systematic uncertainties. The number of reconstructed $\mathrm{t\bar{t}}\gamma$ signal events generated outside the fiducial phase space are scaled with the same value of $r$, i.e., no independent production cross section is assumed for this part of the signal.

The used test statistic is the profiled likelihood ratio, $q(r) = -2\ln L(r, \hat{\theta}_\mathrm{r})/L(\hat{r}, \hat{\theta})$, where $\hat{\theta}_\mathrm{r}$ reflects the values of the nuisance parameters that maximize the likelihood function for a signal strength modifier $r$. The quantities $\hat{r}$ and $\hat{\theta}$ are the values that simultaneously maximize $L$. A multi-dimensional fit is used to extract the observed cross section of the signal process, the nuisance parameters, and the uncertainties in the nuisance parameters [67, 68].

The LM3, LM4p, HM3, HM4p, misDY3 and misDY4p control regions enter the likelihood fit separately for each data-taking period and lepton flavor. In order to extract the $p_\mathrm{T}(\gamma)$ dependence of the background with misidentified electrons, the misDY3 and misDY4p control regions are split into 7 bins separated by the $p_\mathrm{T}(\gamma)$ thresholds 20, 35, 50, 65, 80, 120, and 160 GeV. The LM3, LM4p, HM3, and HM4p regions are similarly separated into 3 bins defined by the $p_\mathrm{T}(\gamma)$ thresholds 20, 65, and 160 GeV. The binning is chosen to obtain a statistical uncertainty in simulated background yields of less than 15%.

The likelihood fit is performed for the inclusive cross section measurements, and separately for the differential measurement. For the extraction of the inclusive cross section, the SR3 and SR4p signal region is divided in three $M_3$ bins in the ranges 0–280, 280–420, and >420 GeV. The binning in $p_\mathrm{T}(\gamma)$, $|\eta(\gamma)|$, and $\Delta R(\ell, \gamma)$ in the SR3 and SR4p signal regions for the differential measurements is provided in Section 9.2. The estimation of contributions from various background processes is performed using control regions binned in $p_\mathrm{T}(\gamma)$, which are used in all inclusive and differential measurements.

## 7 Background estimation

### 7.1 Multijet background

The probability for a multijet event to mimic the final state of the signal process is small and subject to large uncertainties. Therefore, the background from multijet events, comprising events with misidentified and nonprompt leptons, is estimated with a data-based procedure in sideband regions with loosened isolation criteria. For each $N_\mathrm{j}$ requirement, a sideband region is defined by $N_\mathrm{b} = 0$ and requiring the lepton to pass the isolation criterion of the loose lepton working point and to fail the tight lepton selection. The resulting selection is dominated by multijet events. After electroweak backgrounds (W+jets, $\mathrm{t}/\mathrm{t\bar{t}}$, and Drell–Yan) are subtracted based on the expectation from simulation, templates for the distributions of kinematic observables are extracted.

The template normalization is evaluated from a transfer factor (“TF”), defined as the ratio of the multijet event yield with tightly isolated lepton candidates to the yield with loosely isolated lepton candidates. It is obtained in a selection with $N_\mathrm{j} = 2$ and $N_\gamma = 0$ by fitting the distribution of the transverse mass of the W boson candidate, calculated from the formula

$$m_\mathrm{T}(\mathrm{W}) = \sqrt{2 p_\mathrm{T}^{\ell} p_\mathrm{T}^\mathrm{miss} [1 - \cos(\Delta\phi_{\ell,\vec{p}_\mathrm{T}^\mathrm{miss}})]} \quad (1)$$

where $\ell$ indicates the lepton considered in the event. The distribution is taken from data in a $N_\mathrm{b} = 0$ selection with loosely isolated leptons, and electroweak backgrounds are subtracted. The fit is then performed in the selection with tightly isolated leptons where the total normalization of the electroweak background is left floating, while its shape is again taken from simulation. The fit result for the $N_\mathrm{j} = 2$ and $N_\mathrm{b} = 0$ region, including the $m_\mathrm{T}(\mathrm{W})$ multijet distribution from the selection with loosely isolated leptons, is shown in Fig. 3.

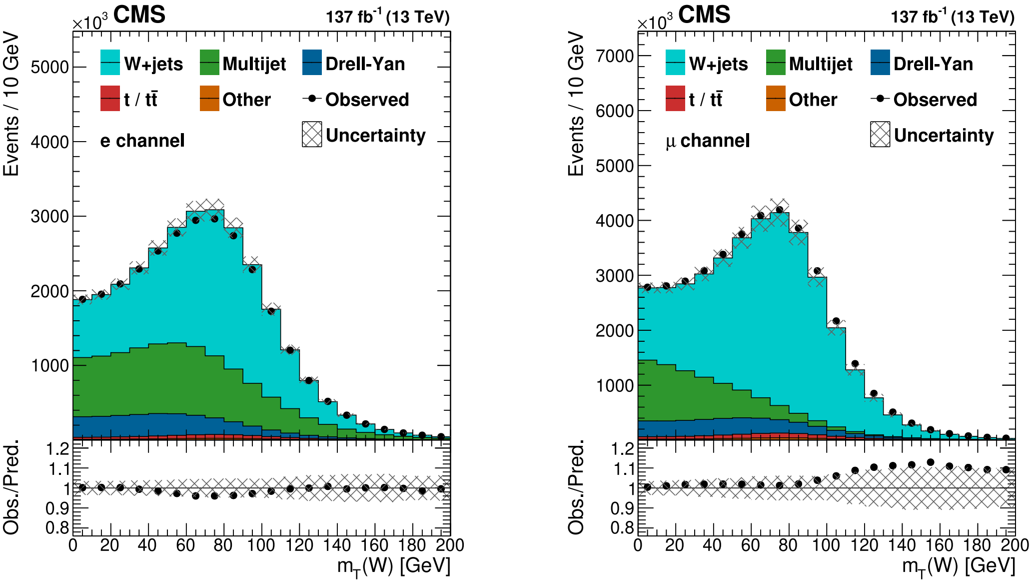

Figure 3: Fit result of the $m_\mathrm{T}(\mathrm{W})$ multijet distribution in the selection with $N_\mathrm{j} = 2$, $N_\mathrm{b} = 0$, and tightly isolated electrons (left) and muons (right). The template obtained from the selection with loosely isolated leptons (green) and the total normalization of the electroweak background are floating in the fit. The lower panels show the ratio of the observed to the predicted event yields. The systematic uncertainties are shown as a hatched band.

Because the efficiency of the tight lepton selection in multijet events depends on $p_\mathrm{T}$ and $\eta$ of the lepton, the estimation procedure, including the TF fit, is performed in a total of 24 bins defined in these observables. Depending on $p_\mathrm{T}$ and $\eta$ of the lepton, the TFs vary in the range of 0.9–3.1 (0.1–0.3) for the e channel and 2.0–3.7 (0.6–1.0) for the $\mu$ channel, for $N_\mathrm{b} = 0$ ($\geq$1). A correction based on simulated multijet events accounts for the TF dependence on $N_\mathrm{j}$. Finally, the multijet estimate is obtained by scaling the $N_\mathrm{b} = 0$ sideband templates with the corresponding TFs and summing the resulting predictions in the 24 bins in lepton $p_\mathrm{T}$ and $\eta$. The total multijet yield is estimated at 12 (8)% in the e ($\mu$) channel in the LM3p, HM3p and misDY3p control regions and below 0.5% in the signal regions.

## 7.2 Nonprompt photon background

The nonprompt photon background component is estimated from data by exploiting the difference between its distribution in the plane defined by the weakly correlated variables $\sigma_{\eta\eta}(\gamma)$ with $I_\mathrm{chg}(\gamma)$, and the corresponding distribution for genuine photons. In a sideband with a requirement of $\sigma_{\eta\eta}(\gamma) \geq 0.011$ on the photon candidate, the expected yields with genuine photons, misidentified electrons, and multijet events are subtracted. The sideband is used to obtain the normalization factor $r_{\mathrm{SB}}$, defined as the ratio of the yield passing the $I_{\mathrm{chg}}(\gamma) < 1.141\,\mathrm{GeV}$ requirement to the event yield failing it. The estimation is obtained by multiplying $r_{\mathrm{SB}}$ with the yield in the normalization region, defined by the nominal $\sigma_{\eta\eta}(\gamma)$ requirement and the inverted criteria on the photon charged hadron isolation, $I_{\mathrm{chg}}(\gamma) > 1.141\,\mathrm{GeV}$. The procedure is carried out separately for lepton flavors, $N_{\mathrm{j}}$ selections, and for each bin of the differential cross section. The deviation from unity of the double-ratio of $r_{\mathrm{SB}}$ to the corresponding ratio in the nominal $\sigma_{\eta\eta}(\gamma)$ selection, stemming from the residual correlation between the two variables, is computed from simulation and it amounts to 18%. This value is used to correct the prediction.

## 7.3 Misidentified electron and genuine photon backgrounds

The background from electrons that are misidentified as photons is obtained from control regions defined by the requirements of $|m(\mathrm{e},\gamma) - m_{\mathrm{Z}}| \leq 10\,\mathrm{GeV}$, and exactly three (misDY3), or four or more (misDY4p) jets. These event samples are enriched by Drell–Yan events with $\mathrm{Z} \to \mathrm{ee}$, where one of the electrons passes the photon selection criteria. The simulated yield of the background component with a misidentified electron is multiplied by the scale factor (SF) defined below, separately for each of the three data-taking periods.

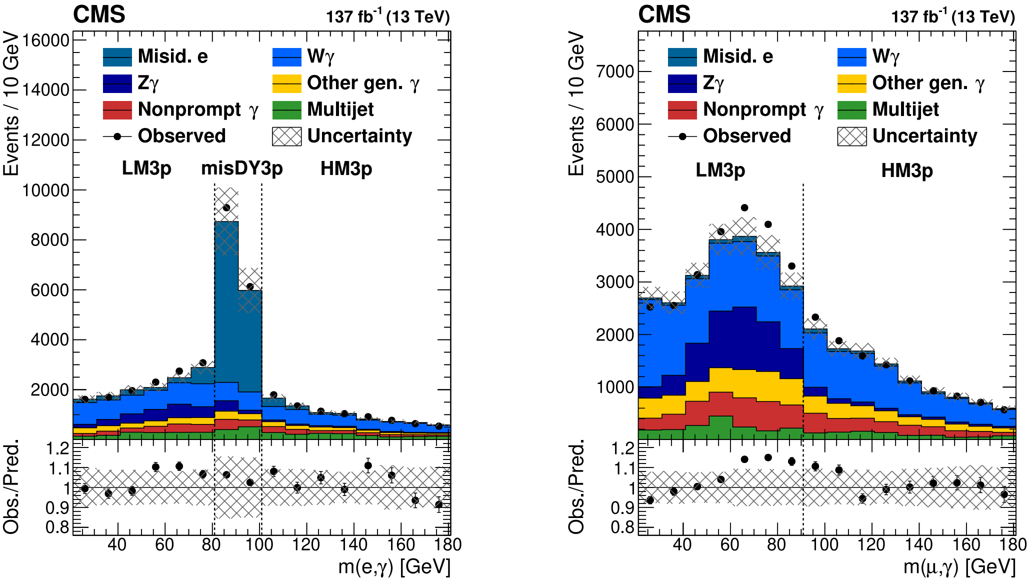

Figure 4: Distribution of the invariant mass of the lepton and the photon, $m(\ell,\gamma)$, in the $N_{\mathrm{j}} \geq 3$, $N_{\mathrm{b}} = 0$ selection for the e channel (left) and the $\mu$ channel (right). The genuine photon contributions of $\mathrm{W}\gamma$ and $\mathrm{Z}\gamma$ are visualized separately. The lower panels show the ratio of the observed to the predicted event yields. The systematic uncertainties are shown as a hatched band.

The SFs for the misidentified electron background and the normalization of the $\mathrm{W}\gamma$ and $\mathrm{Z}\gamma$ processes are obtained from the likelihood fit as described in Section 6.2. The fit includes the data-based multijet estimates and comprises all control regions. The normalization of the $\mathrm{W}\gamma$ process is left floating and the normalization of the $\mathrm{Z}\gamma$ process is allowed to vary within its uncertainty. The resulting $m(\ell,\gamma)$ distributions are shown in Fig. 4 in the $N_{\mathrm{j}} \geq 3$ control regions. The $\mathrm{W}\gamma$ and $\mathrm{Z}\gamma$ processes contribute to the LM3p regions for both lepton flavors. In the HM3p regions, the $\mathrm{W}\gamma$ background is dominant. The background with misidentified electrons is dominant in the misDY3 and misDY4p regions close to the $m_{\mathrm{Z}}$ peak. A correction of 15% to the normalization of the Drell–Yan process is measured in a data sample with two well-identified leptons satisfying $|m(\ell,\ell) - m_{\mathrm{Z}}| \leq 10\,\mathrm{GeV}$ and $N_{\mathrm{j}} \geq 3$, and is included in these results. A summary of the extracted SF for the misidentified electron background and the normalization of the $\mathrm{Z}\gamma$ and $\mathrm{W}\gamma$ processes is provided in Table 4. The observed changes in the SF for misidentified electrons are a result of the pixel detector replacement in 2017 and its operating conditions in the three data-taking periods. The stability of the procedure to estimate the yields of misidentified electrons and genuine photons is assessed by repeating the fit on individual data-taking periods, separately for the $N_{\mathrm{j}} = 3$ and $\geq$4 selections, and separately for the lepton flavors. The extracted SFs from these checks agree within the uncertainties.

Table 4: Extracted SFs for the contribution from misidentified electrons for the three data-taking periods and for the normalization of the $\mathrm{Z}\gamma$ and $\mathrm{W}\gamma$ background components obtained from the likelihood fit.

| Scale factor | Value |
|---|---|
| Misidentified electrons (2016) | $2.22 \pm 0.28$ |
| Misidentified electrons (2017) | $1.83 \pm 0.24$ |
| Misidentified electrons (2018) | $1.59 \pm 0.18$ |
| $\mathrm{Z}\gamma$ normalization | $0.83 \pm 0.10$ |
| $\mathrm{W}\gamma$ normalization | $1.20 \pm 0.09$ |

## 8 Systematic uncertainties

The systematic uncertainties affecting the signal selection efficiency and background yields are summarized in Table 5. The table shows the range of variations in the different bins of the analysis caused by each systematic uncertainty in the signal and background yields, as well as an estimate of the impact of each uncertainty in the measured inclusive cross section. The table also indicates whether the uncertainties are treated as uncorrelated or fully correlated among the data-taking periods.

The integrated luminosities of the 2016, 2017, and 2018 data-taking periods are individually known with uncertainties in the 2.3–2.5% range [69–71], while the total Run 2 (2016–2018) integrated luminosity has an uncertainty of 1.8%, the improvement in precision reflecting the (uncorrelated) time evolution of some systematic effects. The uncertainty in the inclusive cross section from these sources is, therefore, 1.8%. Simulated events are reweighted according to the distribution of the number of interactions in each bunch crossing corresponding to a total inelastic pp cross section of 69.2 mb [52]. The uncertainty in the total inelastic pp cross section is 4.6% [72] and affects the pileup estimate. The uncertainty due to the pileup effect is about 2% for the expected yields and less than 0.5% for the inclusive cross section.

The uncertainties in the SFs used to match the simulated trigger selection efficiencies to the ones observed in data are propagated to the results. From the "tag-and-probe" measurement [55, 58], an uncertainty of up to 0.5% is assigned to the yields obtained in simulation. Lepton selection efficiencies are measured in bins of lepton $p_{\mathrm{T}}$ and $\eta$, and are found to be in the range 50–80 (75–85)% for electrons (muons). These measurements are performed separately in data and simulation and their ratio is used to scale the yields obtained in the simulation. The impact of these uncertainties on the inclusive cross section is 0.5 (0.7)% for the electron (muon) channel.

In the barrel section of the ECAL, an energy resolution of about 1% is achieved for uncon-

Table 5: Breakdown of the total uncertainty in its statistical and systematic components. The first column indicates the source of the uncertainty. The second column shows the correlation between the data-taking periods. The third column shows the typical pre-fit uncertainties in the total simulated yields in the signal region. The last column gives the corresponding systematic uncertainty in the $\mathrm{t\bar{t}}\gamma$ cross section from the fit to the data.

| | Source | Correlation | Uncertainty [%] | |
|---|---|---|---|---|
| | | | yield | $\sigma(\mathrm{t\bar{t}}\gamma)$ |
| **Experimental** | Integrated luminosity | partial | 2.3–2.5 | 1.8 |
| | Pileup | 100% | 0.5–2.0 | <0.5 |
| | Trigger efficiency | — | <0.5 | <0.5 |
| | Electron reconstruction and identification | 100% | 0.2–1.7 | <0.5 |
| | Muon reconstruction and identification | partial | 0.5–0.7 | 0.7 |
| | Photon reconstruction and identification | 100% | 0.4–1.4 | 1.0 |
| | $p_{\mathrm{T}}(\mathrm{e})$ and $p_{\mathrm{T}}(\gamma)$ reconstruction | 100% | 0.1–1.2 | <0.5 |
| | JES | partial | 1.0–4.1 | 1.9 |
| | JER | — | 0.4–1.6 | 0.6 |
| | b tagging | 100% (2017/2018) | 0.8–1.6 | 1.1 |
| | L1 prefiring | 100% (2016/2017) | 0.3–0.9 | <0.5 |
| **Theoretical** | Tune | 100% | 0.1–1.9 | <0.5 |
| | Color reconnection | 100% | 0.4–3.6 | 0.6 |
| | ISR/FSR | 100% | 1.0–5.6 | 1.9 |
| | PDF | 100% | <0.5 | <0.5 |
| | ME scales $\mu_{\mathrm{R}}$, $\mu_{\mathrm{F}}$ | 100% | 0.4–4.7 | <0.5 |
| **Background** | Multijet normalization | 100% | 1.3–6.5 | 0.9 |
| | Nonprompt photon background | 100% | 1.2–2.7 | 2.0 |
| | Misidentified e | — | 2.5–8.0 | 1.8 |
| | $\mathrm{Z}\gamma$ normalization | 100% | 0.6–2.5 | 0.5 |
| | $\mathrm{W}\gamma$ normalization | 100% | 1.0–3.5 | 2.4 |
| | DY normalization | 100% | 0.1–1.1 | 1.0 |
| | $\mathrm{t\bar{t}}$ normalization | 100% | 1.0–1.9 | 1.0 |
| | "Other" bkg. normalization | 100% | 0.3–1.0 | <0.5 |
| | Total systematic uncertainty | | | 5.7 |
| | Statistical uncertainty | | | 0.9 |
| | Total | | | 5.8 |

verted or late-converting highly energetic photons in the tens of GeV energy range. The energy resolution of the remaining barrel photons is about 1.3% up to $|\eta| = 1$, changing to about 2.5% at $|\eta| = 1.4$ [56]. Uncertainties in the photon energy scale and resolution are measured with electrons from Z boson decays, reconstructed using information exclusively from the ECAL [56, 57]. Additionally, an event sample enriched in $\mu^+\mu^-\gamma$ events is used to measure an SF correcting the efficiency of the electron veto [73]. The total uncertainty in the photon energy and identification amounts to 1.4% for the inclusive cross section, and reaches 2% for $p_{\mathrm{T}}(\gamma) > 100\,\mathrm{GeV}$.

Uncertainties in the jet energy calibration are estimated by shifting the jet energy corrections in simulation up and down by one standard deviation. Depending on $p_{\mathrm{T}}$ and $\eta$, the uncertainty in JES varies in the range 2–5% [61], leading to uncertainties in the predicted signal and background yields of 1.0–4.1% and an impact on the inclusive cross section of 1.9%. For the signal and background processes modeled via simulation, the uncertainty in the measurement is determined from the observed differences in the yields with and without the shift in jet energy corrections. The same technique is used to calculate the uncertainties from the JER, which are found to be less than 1% [61]. The b tagging efficiency in the simulation is corrected using SFs determined from data [62, 74]. These are estimated separately for correctly and incorrectly identified jets, and each results in an uncertainty of about 0.8–1.6% in the yields in the signal regions, depending on $N_{\mathrm{b}}$.

During the 2016 and 2017 data-taking periods, a gradual shift in the timing of the inputs of the ECAL L1 trigger in the forward endcap region ($|\eta| > 2.4$) led to a specific inefficiency (labeled "L1 prefiring" in Table 5). A correction for this effect was determined using an unbiased data sample and is found to be relevant in events with jets with $2.4 < |\eta| < 3.0$ and $p_{\mathrm{T}} > 100\,\mathrm{GeV}$. While no reconstructed objects at this $\eta$ directly enter the measurements, it can affect the $p_{\mathrm{T}}^{\mathrm{miss}}$ observable. A systematic variation of 20% of this correction for affected objects leads to an uncertainty of 0.3–0.9% in the predicted yields.

To estimate the theoretical uncertainties from missing higher-order corrections in the signal cross section calculation, the choice of $\mu_{\mathrm{R}}$ and $\mu_{\mathrm{F}}$ are varied independently up and down by a factor of 2, ignoring the case in which one parameter is scaled up while the other is scaled down. The envelope of the acceptance variations is taken as the systematic uncertainty in each bin before the profiled likelihood fit and is found to be smaller than 4.7%. The different sets in the NNPDF PDF [48] are used to estimate the corresponding uncertainty in the acceptance for the cross section measurement, which is less than 0.5%. The scale, PDF, and $\alpha_{\mathrm{S}}$ uncertainties in the inclusive fiducial cross section of the $\mathrm{t\bar{t}}\gamma$ process, evaluated with MADGRAPH5_aMC@NLO at NLO in QCD, amount to 17.5%.

In the parton shower simulation, the uncertainty from the choice of $\mu_{\mathrm{F}}$ is estimated by varying the scale of initial- and final-state radiation (ISR/FSR) up and down by factors of 2 and $\sqrt{2}$, respectively, as suggested in Ref. [44]. The default configuration in PYTHIA includes a model of color reconnection based on multiple parton interactions (MPI) with early resonance decays switched off. To estimate the uncertainty from this choice of model, the analysis is repeated with three other color reconnection schemes within PYTHIA: the MPI-based scheme with early resonance decays switched on, a gluon-move scheme [75], and a QCD-inspired scheme [76]. The total uncertainty from color reconnection modeling is estimated by taking the maximum deviation from the nominal result and amounts to 0.6% in the inclusive cross section.

The uncertainty in the normalization of the QCD multijet component is based on the variation of the TF with $N_{\mathrm{j}}$ for different $N_{\mathrm{b}}$ and amounts to 50%. Independent uncertainties are considered for the contributions to the $N_{\mathrm{b}} = 0$ and $\geq 1$ yields. These have a significant impact only in the LM3, LM4p, HM3, and HM4p control regions, and lead to an uncertainty of 0.9% in the measured inclusive cross section.

The uncertainty in the nonprompt photon prediction is based on the modelling of the $I_{\mathrm{chg}}(\gamma)$ distribution for different requirements on $\sigma_{\eta\eta}(\gamma)$ and leads to an uncertainty of 2% in the inclusive cross section. The normalization of the W$\gamma$ process is left floating in the profiled likelihood. To account for the uncertainty in the $N_{\mathrm{j}}$ modelling of the Z$\gamma$ process, we include an uncertainty of 30% in its normalization. Moreover, 40 (20)% uncertainty is assigned to the normalization of the Z$\gamma$ (W$\gamma$ and misidentified electron) background in the $N_{\mathrm{j}} \geq 4$ signal and control regions. The corresponding impact of the normalization of the Z$\gamma$ and W$\gamma$ contributions are 0.5 and 2.4%, respectively. The component with misidentified electrons leads to an uncertainty of up to 8% in the predicted background yields with an impact on the inclusive cross section of 1.8%. The 8% uncertainty in the normalization of the Drell–Yan process, the 5% uncertainty in the $\mathrm{t\bar{t}}$ normalization, and the uncertainties in the normalization of other small background components lead to additional uncertainties below 1%.

# 9 Results

## 9.1 Inclusive cross section measurement

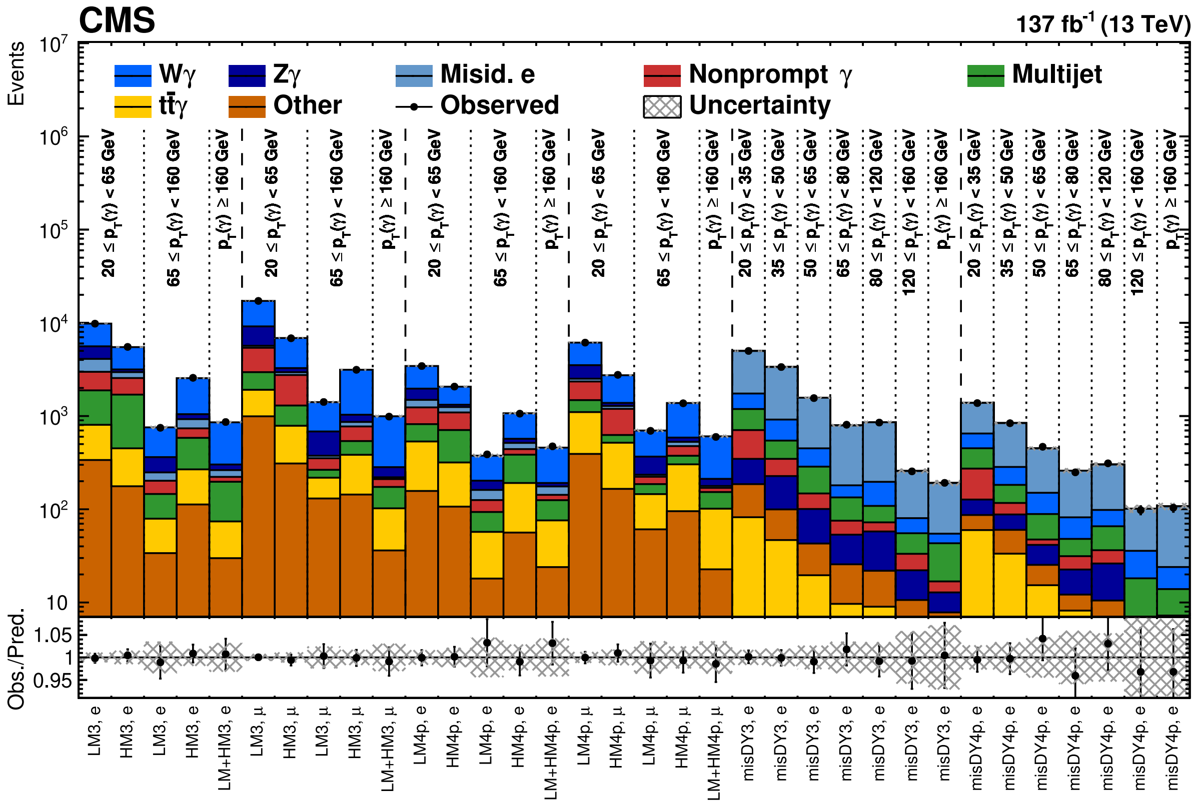

Figure 5: Fitted and observed yields in the LM3, LM4p, HM3, HM4p, misDY3, and misDY4p control regions using the post-fit values of the nuisance parameters. The lower panel shows the ratio of the observed to the predicted event yields. The hatched band shows the systematic uncertainty in the background prediction.

The observed data, as well as the predicted signal and background yields in the control and signal regions resulting from the likelihood fit, are shown in Figs. 5 and 6. The signal cross section is extracted from these categories using the statistical procedure detailed in Section 6.2.

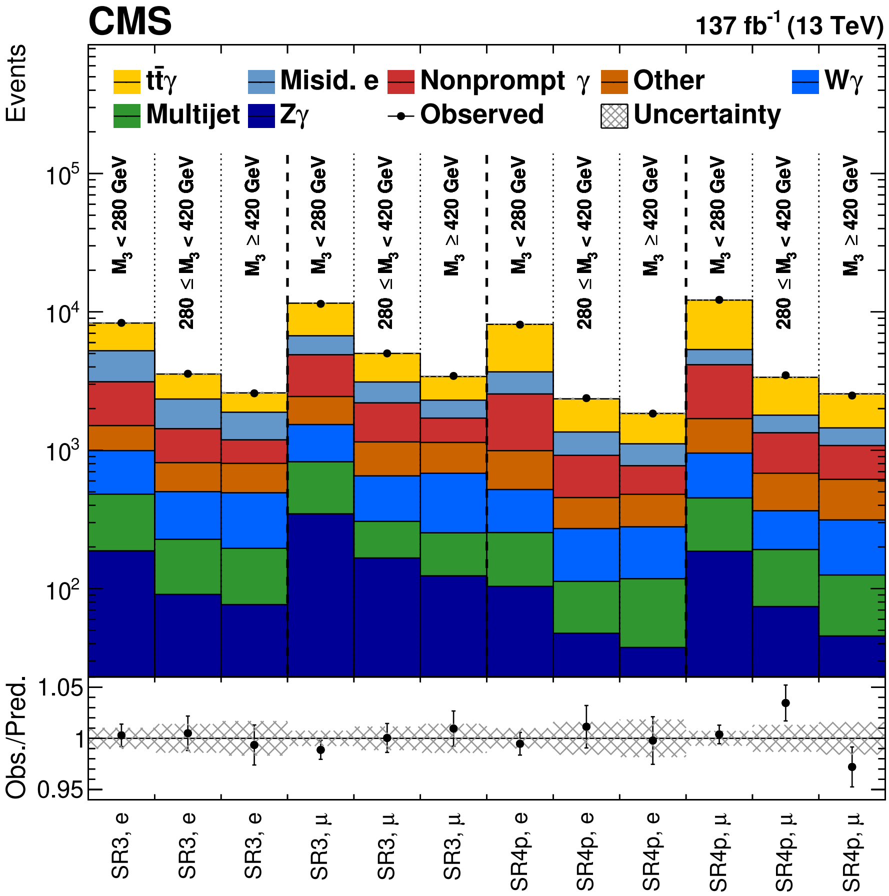

Figure 6: Fitted and observed yields in the SR3 and SR4p signal regions using the post-fit values of the nuisance parameters. The lower panel shows the ratio of the observed to the predicted event yields. The systematic uncertainties are shown as a hatched band.

In the fit, nuisance parameters for the various systematic uncertainties and the normalization of background processes, as described in Section 8, are included. Besides the extraction of the nuisance parameters related to normalization of the misidentified electron component and the $Z\gamma$ and $W\gamma$ backgrounds, there are no significant constraints of other nuisance parameters. Using three bins in $M_3$ reduces the uncertainty in the backgrounds without a hadronically decaying top quark, e.g., the misidentified electron background and the $W\gamma$ and $Z\gamma$ processes. The reduction of the total uncertainty in the inclusive cross section is 1%. The normalization of the $W\gamma$ background is the largest individual contribution to the uncertainty in the inclusive cross section measurement and amounts to 2.4%.

The combined inclusive cross section of the $N_\mathrm{j} = 3$ and $\geq 4$ channels within the fiducial phase space is measured to be

$$\sigma(\mathrm{t\bar{t}}\gamma) = 800 \pm 7\,(\mathrm{stat}) \pm 46\,(\mathrm{syst})\,\mathrm{fb} \qquad (2)$$

in good agreement with the SM expectation of $\sigma^{\mathrm{NLO}}(\mathrm{t\bar{t}}\gamma) = 773 \pm 135\,\mathrm{fb}$. The measured value of the signal strength modifier is

$$r = 1.034 \pm 0.009\,(\mathrm{stat}) \pm 0.059\,(\mathrm{syst}). \qquad (3)$$

A comparison of the measured cross sections and the SM prediction is shown in Fig. 7 for all measurements split according to the $N_\mathrm{j}$ and the lepton flavor.

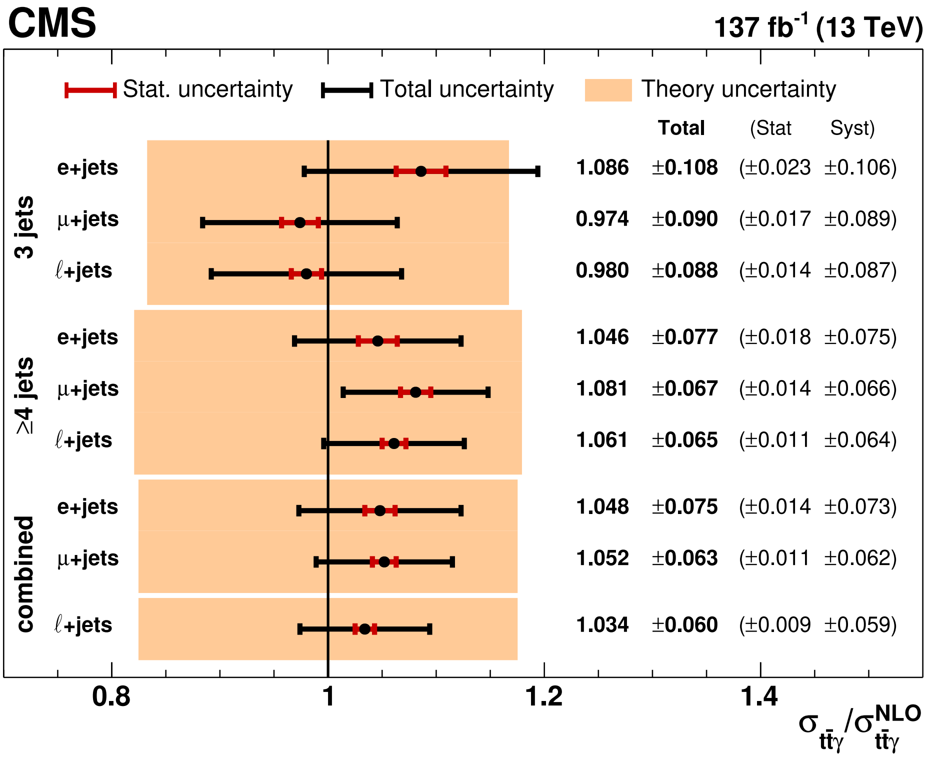

Figure 7: Summary of the measured cross section ratios with respect to the NLO cross section prediction for $N_{\mathrm{j}} = 3$, $\geq 4$, and combined signal regions in the electron channel, muon channel, and the combined single-lepton channel. The orange band indicates the theory uncertainty in the prediction.

## 9.2 Differential cross section measurement

The differential cross section is measured as a function of $p_{\mathrm{T}}(\gamma)$, $|\eta(\gamma)|$, and $\Delta R(\ell, \gamma)$. Results are obtained simultaneously for the electron and muon channels, the 3 jet and $\geq$4 jet bins, and for the three data-taking periods. The binning in the SR3 and SR4p selections for the measurement of the differential distributions at the reconstruction level is shown in Table 6.

Table 6: Binning choices in the differential measurements at the reconstruction level.

| | |
|---|---|
| $p_{\mathrm{T}}(\gamma)$ | 20, 35, 50, 65, 80, 100, 120, 140, 160, 200, 260, $\geq$320 GeV |
| $\lvert\eta(\gamma)\rvert$ | 0, 0.15, 0.30, 0.45, 0.60, 0.75, 0.90, 1.05, 1.20, 1.35, 1.4442 |
| $\Delta R(\ell, \gamma)$ | 0.4, 0.6, 0.8, 1.0, 1.2, 1.4, 1.6, 1.8, 2.0, 2.2, 2.4, 2.6, 2.8, $\geq$3.0 |

As described in Section 6.2, the same control regions are used for the inclusive and differential cross section measurements. The signal strength is left floating in the profiled likelihood fit separately for each of the differential bins, the $N_{\mathrm{j}}$ selection, the lepton flavor, and the data-taking period. The fit is performed separately for each differential distribution.

The distributions of the observables after background subtraction are further unfolded to the fiducial particle level phase space defined in Section 5. The unfolded differential cross section is defined in the same phase space as the inclusive cross section reported above, i.e., in the phase space where the top quark pair is produced in association with a photon satisfying $p_{\mathrm{T}}(\gamma) > 20\,\mathrm{GeV}$ and $|\eta(\gamma)| < 1.4442$. Signal events that are not generated within the fiducial region amount to 5–10% and are subtracted based on simulation. In the simulation, $p_{\mathrm{T}}(\gamma)$ is taken as the transverse momentum after accounting for the effects of QCD and electroweak radiation.

The $\mathrm{t\bar{t}}\gamma$ MADGRAPH5_aMC@NLO MC sample is used to construct a response matrix that takes into account both detector response and acceptance corrections. The same corrections, SFs, and uncertainties as used in the inclusive cross section are applied. Because of the high momentum- and angular resolutions of photons and leptons, the fraction of events migrating from a specific momentum region at the particle level to another one at the reconstruction level is small for all unfolded distributions. Under such conditions, and with the chosen bin size, no regularization term is required [77]. The TUNFOLD package [78] is used to obtain the results for the three measured observables using matrix inversion. The binning in the fiducial region is chosen such that two bins at the reconstruction level correspond to one bin in the fiducial region for most cases. This choice provides stability to the unfolding algorithm.

Uncertainties in the estimated signal yields are propagated through the unfolding procedure, including the effects on the response matrix. Experimental uncertainties from the detector response and efficiency, such as the photon identification, JES, and b tagging uncertainties, are applied as a function of the reconstructed observable. The differential cross sections, obtained by this procedure, are shown in Fig. 8. It includes a comparison with simulation obtained from MADGRAPH5_aMC@NLO interfaced to HERWIG++ [79] v2.7.1 with the EE5C tune [45] and to HERWIG7 v7.1.4 with the CH3 tune [80] for the parton shower and hadronization. The inclusive fiducial cross section predicted by HERWIG++ (HERWIG7) is 8.3% (5.4%) lower than for the nominal simulation.

The bin efficiency, defined as the fraction of generated events that are reconstructed in the corresponding bins at reconstruction level, is in the range of 20–30%. The bin purity, defined as the fraction of reconstructed events that originate from the corresponding bin at the particle level, is in the range of 85–90%. For $p_{\mathrm{T}}(\gamma) > 120\,\mathrm{GeV}$, the uncertainties in the JES, the photon identification efficiency, and the color reconnection modeling are the largest sources of systematic uncertainty. The correlation matrices of the systematic uncertainties for the unfolded differential measurements are shown in Fig. 9. The correlations are lower in the tail of $p_{\mathrm{T}}(\gamma)$ due to larger statistical uncertainties in the simulation. The first bin of the $\Delta R(\ell,\gamma)$ measurement is less affected by uncertainties in the normalization of backgrounds, resulting in slightly lower correlations in this case. All correlations from statistical uncertainties originating from the data are below 7%. Including the uncertainty in the fiducial signal cross section, we perform a compatibility test of the unfolded distribution and the nominal prediction. The corresponding $\chi^2$ test statistic evaluates to 12.5 with 9 degrees of freedom (dof) for the $p_{\mathrm{T}}(\gamma)$ distribution, 5.2 with 5 dof for $|\eta(\gamma)|$, and 6.3 with 7 dof for $\Delta R(\ell,\gamma)$.

## 9.3 Effective field theory interpretation

Many BSM models predict anomalous couplings of the top quark to the electroweak gauge bosons [81–87]. The differential cross section measurement is interpreted at the reconstruction level in SM-EFT in the Warsaw basis [88], formed by 59 baryon number conserving dimension-six Wilson coefficients. Among them, 15 are relevant for top quark interactions [89]. Anomalous interactions between the top quark and the gluon (chromomagnetic and chromoelectric dipole moment interactions) are tightly constrained by the $\mathrm{t\bar{t}}$+jets measurements [90, 91]. Similarly, the modification of the Wtb vertex is best constrained by measurements of the W helicity fractions in top quark pair production [92] and in $t$-channel single top quark production [93].

The Wilson coefficients in the Warsaw basis inducing electroweak dipole moments are denoted by $C_{\mathrm{uB}}^{(33)}$ and $C_{\mathrm{uW}}^{(33)}$ [12]. The SM gauge symmetry provides the $\mathrm{t\bar{t}Z}$ and the $\mathrm{t\bar{t}}\gamma$ final states with

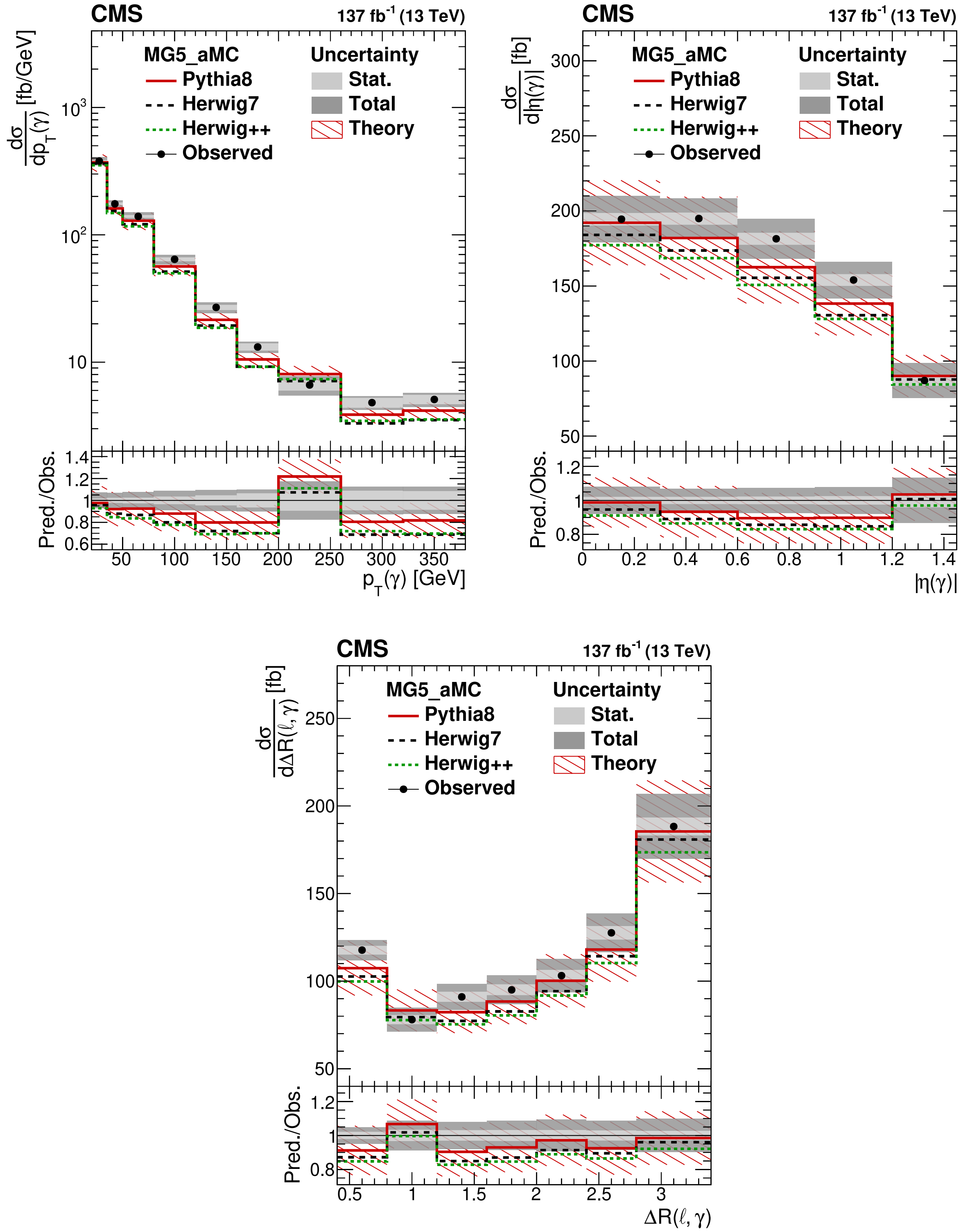

Figure 8: The unfolded differential cross sections for $p_{\mathrm{T}}(\gamma)$ (upper left), $|\eta(\gamma)|$ (upper right), and $\Delta R(\ell,\gamma)$ (lower) compared with simulation obtained from the MADGRAPH5_aMC@NLO event generator interfaced to PYTHIA (red, solid), HERWIG7 (black, dashed) and HERWIG++ (green, dotted) for the parton shower and hadronization. For $p_{\mathrm{T}}(\gamma)$ and $\Delta R(\ell,\gamma)$, the last bin includes the overflow. The lower panel displays the ratio of simulation to the observation. The inner and outer bands show the statistical and total uncertainties, respectively. Photons radiated from leptons and satisfying $\Delta R(\ell,\gamma) > 0.4$ are included in the signal and contribute significantly to the first bin of the differential $\Delta R(\ell,\gamma)$ cross section.

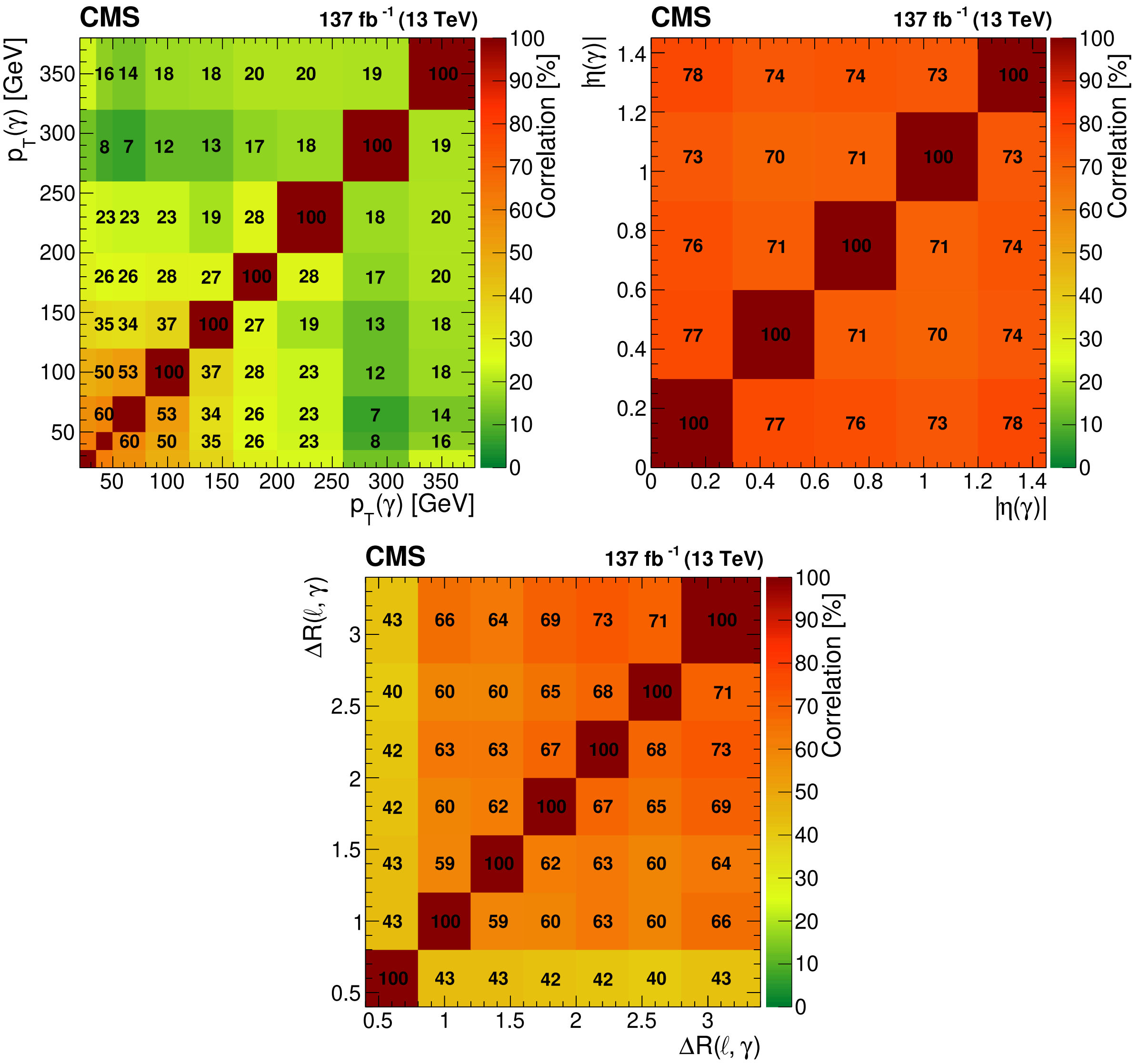

Figure 9: The correlation matrices of systematic uncertainties for the unfolded differential measurement for $p_T(\gamma)$ (upper left), $|\eta(\gamma)|$ (upper right), and $\Delta R(\ell, \gamma)$ (lower).

complementary constraining power [1–4]. The linear relations

$$\begin{aligned}
c_{\mathrm{tZ}} &= \mathrm{Re}\left(-\sin\theta_{\mathrm{W}} C_{\mathrm{uB}}^{(33)} + \cos\theta_{\mathrm{W}} C_{\mathrm{uW}}^{(33)}\right),\\
c_{\mathrm{tZ}}^{\mathrm{I}} &= \mathrm{Im}\left(-\sin\theta_{\mathrm{W}} C_{\mathrm{uB}}^{(33)} + \cos\theta_{\mathrm{W}} C_{\mathrm{uW}}^{(33)}\right),\\
c_{\mathrm{t}\gamma} &= \mathrm{Re}\left(\cos\theta_{\mathrm{W}} C_{\mathrm{uB}}^{(33)} + \sin\theta_{\mathrm{W}} C_{\mathrm{uW}}^{(33)}\right),\\
c_{\mathrm{t}\gamma}^{\mathrm{I}} &= \mathrm{Im}\left(\cos\theta_{\mathrm{W}} C_{\mathrm{uB}}^{(33)} + \sin\theta_{\mathrm{W}} C_{\mathrm{uW}}^{(33)}\right),
\end{aligned}$$

express the modifications of the $\mathrm{t\bar{t}Z}$ interaction vertex, $c_{\mathrm{tZ}}$ and $c_{\mathrm{tZ}}^{\mathrm{I}}$, and of the $\mathrm{t\bar{t}}\gamma$ interaction vertex, $c_{\mathrm{t}\gamma}$ and $c_{\mathrm{t}\gamma}^{\mathrm{I}}$, in the Warsaw basis. The constraint $C_{\mathrm{uW}}^{(33)} = 0$ ensures a SM Wtb vertex. Under this assumption, $c_{\mathrm{tZ}}$ ($c_{\mathrm{tZ}}^{\mathrm{I}}$) and $c_{\mathrm{t}\gamma}$ ($c_{\mathrm{t}\gamma}^{\mathrm{I}}$) are dependent and we choose the former to parametrize the BSM hypothesis.

The spectrum of $p_{\mathrm{T}}(\gamma)$ is a sensitive probe to such modifications. Other observables, e.g., $|\eta(\gamma)|$ or $\Delta R(\ell,\gamma)$, are found to be largely insensitive. Wilson coefficients that are not considered in this work are kept at their SM values and the SM-EFT expansion parameter is set to a mass scale $\Lambda = 1\,\mathrm{TeV}$. Using the SM-EFT parametrization from Ref. [12], simulated samples at the particle level are produced with non-zero values of the Wilson coefficients $c_{\mathrm{tZ}}$ and $c_{\mathrm{tZ}}^{\mathrm{I}}$. The $\mathrm{t\bar{t}}\gamma$ signal process and all background processes affected by $c_{\mathrm{tZ}}$ or $c_{\mathrm{tZ}}^{\mathrm{I}}$ at the ME level are included in the simulation. These samples are used to reweight the nominal simulation in the fiducial phase space using the quadratic parametrization detailed in Ref. [94]. The reweighting procedure is validated for a reduced set of samples at non-zero values of $c_{\mathrm{tZ}}$ and $c_{\mathrm{tZ}}^{\mathrm{I}}$ and excellent agreement is found.

The SR3 and SR4p signal regions and the $p_{\mathrm{T}}(\gamma)$ boundaries defining the bins in Table 6 are used to construct a binned likelihood function $L(\theta)$ as a product of Poisson probabilities from the yields in the signal and control regions. The nuisance parameters are labeled by $\theta$ and the profile likelihood ratio $q = -2\ln(L(\hat{\theta},\vec{C})/L(\hat{\theta}_{\mathrm{max}}))$ is the test statistic. Here, $\hat{\theta}$ is the set of nuisance parameters maximizing the likelihood function at a BSM point defined by the Wilson coefficients collectively denoted by $\vec{C}$. In the denominator, $\hat{\theta}_{\mathrm{max}}$ maximizes the likelihood function in the BSM parameter space. The $\mathrm{t\bar{t}}\gamma$ signal is normalized according to the SM expectation at NLO in QCD and its uncertainty is included as a nuisance.

Figure 10 shows the result of the fit for the SR3 and SR4p signal regions and separately for each lepton flavor. No deviations from the SM expectations are observed. The best fit point is found at $(c_{\mathrm{tZ}}, c_{\mathrm{tZ}}^{\mathrm{I}}) = (-0.25, -0.08)$ and the corresponding spectrum is overlaid together with the ones from several other choices for non-zero values of the Wilson coefficients. Figure 11 displays the one-dimensional scans of the coefficients. In the upper row, one Wilson coefficient is scanned, while the other is profiled. The lower row shows the scans, where the second Wilson coefficient is set to zero. The second local minima in the scans of the log-likelihood as a function of $c_{\mathrm{tZ}}$ and $c_{\mathrm{tZ}}^{\mathrm{I}}$, visible in Fig. 11 (lower row), is the result of a mild tension with the SM hypothesis in conjunction with the similarity of the predictions for Wilson coefficients with opposite sign. The corresponding one-dimensional intervals at 68 and 95% confidence interval (CL) are listed in Table 7 and are more stringent than previous limits obtained from $\mathrm{t\bar{t}Z}$ final states [95, 96]. Models with non-zero electroweak dipole moments predict a harder $p_{\mathrm{T}}(\gamma)$ spectrum that is not observed in data. Figure 12 shows the best fit result in the two-dimensional plane spanned by $c_{\mathrm{tZ}}$ and $c_{\mathrm{tZ}}^{\mathrm{I}}$ and the log-likelihood scan. The SM prediction is within the 95% CL of the best fit value of the $c_{\mathrm{tZ}}$ and $c_{\mathrm{tZ}}^{\mathrm{I}}$ coefficients.

In Fig.13, the 95% CL intervals are compared with the previous CMS results based on the inclusive [97] and differential [95] $\mathrm{t\bar{t}Z}$ cross section measurement, a CMS result based on $\mathrm{t\bar{t}}$ in final states with additional leptons [94], and the most recent ATLAS result [96] (lower). The result of a global SM-EFT analysis, including results from Ref. [95], is also shown [98]. The present result improves upon the previous constraints by about a factor of 2.5.

Table 7: Summary of the one-dimensional intervals at 68 and 95% CL.

| | Wilson coefficient | | 68% CL interval $(\Lambda/\,\mathrm{TeV})^2$ | 95% CL interval $(\Lambda/\,\mathrm{TeV})^2$ |
|---|---|---|---|---|
| Expected | $c_{\mathrm{tZ}}$ | $c^{\mathrm{I}}_{\mathrm{tZ}} = 0$ | $[-0.19, 0.21]$ | $[-0.29, 0.32]$ |
| | | profiled | $[-0.19, 0.21]$ | $[-0.29, 0.32]$ |
| | $c^{\mathrm{I}}_{\mathrm{tZ}}$ | $c_{\mathrm{tZ}} = 0$ | $[-0.20, 0.20]$ | $[-0.30, 0.31]$ |
| | | profiled | $[-0.20, 0.20]$ | $[-0.30, 0.31]$ |
| Observed | $c_{\mathrm{tZ}}$ | $c^{\mathrm{I}}_{\mathrm{tZ}} = 0$ | $[-0.35, -0.16]$ | $[-0.42, 0.38]$ |
| | | profiled | $[-0.35, 0.07]$ | $[-0.42, 0.39]$ |
| | $c^{\mathrm{I}}_{\mathrm{tZ}}$ | $c_{\mathrm{tZ}} = 0$ | $[-0.35, -0.16], [0.17, 0.35]$ | $[-0.42, 0.42]$ |
| | | profiled | $[-0.32, 0.31]$ | $[-0.41, 0.41]$ |

## 10 Summary

A measurement of the cross section for the top quark pair production in association with a photon using a data sample of proton-proton collisions at $\sqrt{s} = 13\,\mathrm{TeV}$, corresponding to an integrated luminosity of $137\,\mathrm{fb}^{-1}$, collected with the CMS detector at the LHC has been presented. It is the first result of the CMS Collaboration on measurements in the $\mathrm{t\bar{t}}\gamma$ final state using 13 TeV data. The analysis has been performed in the single-lepton channel with events with exactly three and four or more jets among which at least one is b tagged. Background components with misidentified electrons, photons originating in the hadronization of jets, the multijet component, and prompt photons from the $\mathrm{W}\gamma$ and $\mathrm{Z}\gamma$ processes are estimated from data. The measured inclusive cross section in a fiducial region with photon transverse momentum $p_{\mathrm{T}}(\gamma) > 20\,\mathrm{GeV}$ and jet multiplicity greater than 3 is measured to be $800 \pm 7\,\mathrm{(stat)} \pm 46\,\mathrm{(syst)}\,\mathrm{fb}$, in good agreement with the standard model prediction at next-to-leading order in quantum chromodynamics.

Differential cross sections for $p_{\mathrm{T}}(\gamma)$ and absolute value of the photon pseudorapidity, as well as for the angular separation of the lepton and the photon, have been measured and unfolded to particle level in the same fiducial volume. The comparison to simulation was performed using different showering algorithms. The measurements are also interpreted in terms of limits on the Wilson coefficients in the context of the standard model effective field theory. The confidence intervals for the Wilson coefficients $c_{\mathrm{tZ}}$ and $c^{\mathrm{I}}_{\mathrm{tZ}}$ are the most stringent to date.

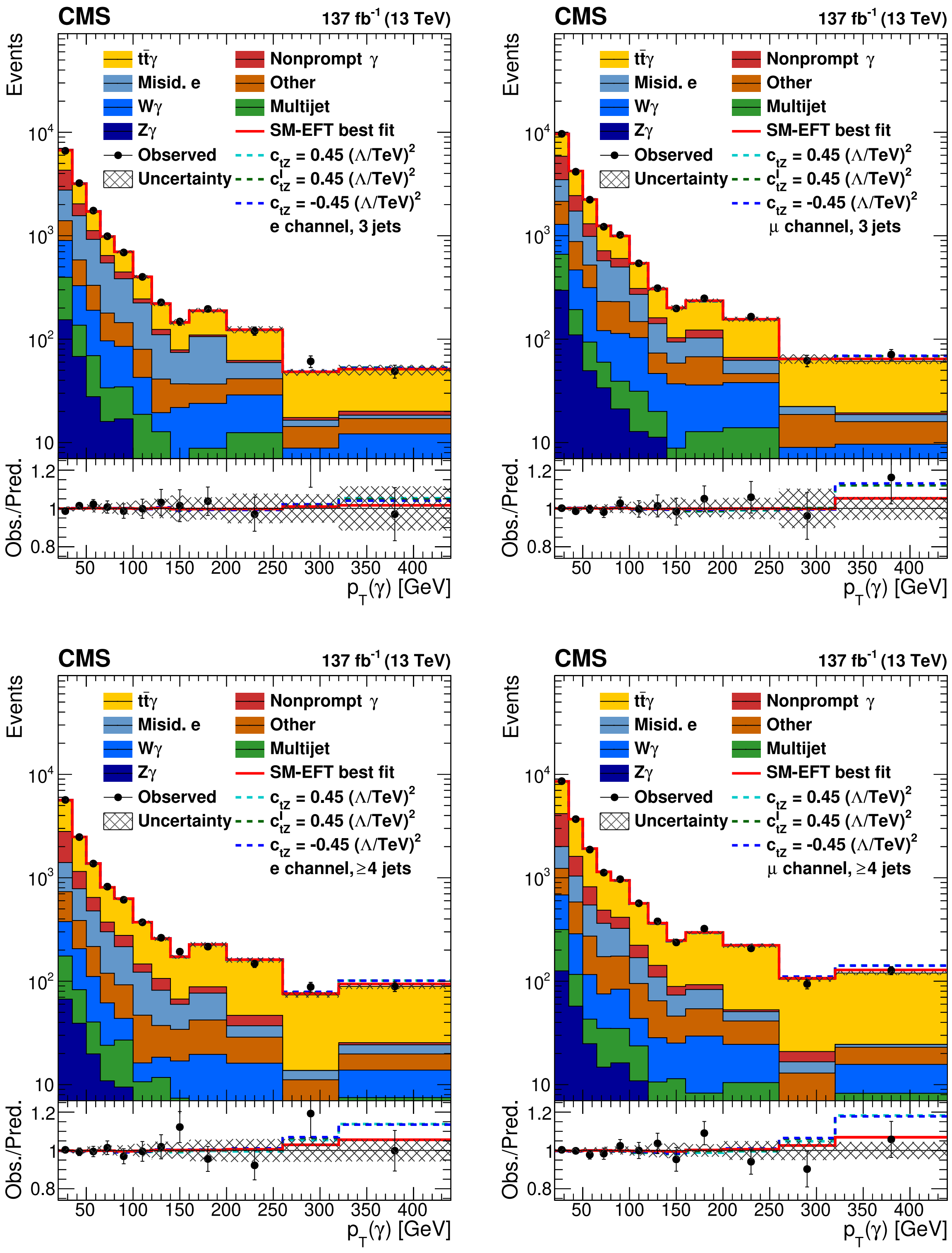

Figure 10: The observed (points) and predicted (shaded histograms) post-fit yields for the combined Run 2 data set in the SR3 (upper) and SR4p (lower) signal regions for the electron (left) and muon channel (right). The vertical bars on the points give the statistical uncertainties in the data. The lower panel displays the ratio of the data to the predictions and the hatched regions show the total uncertainty. The solid line shows the SM-EFT best fit prediction and the dashed lines show different predictions for non-zero Wilson coefficients, $c_{tZ} = 0.45$ (light blue), $c^I_{tZ} = 0.45$ (green), and $c_{tZ} = -0.45$ (dark blue), where $\Lambda$ is set to 1 TeV.

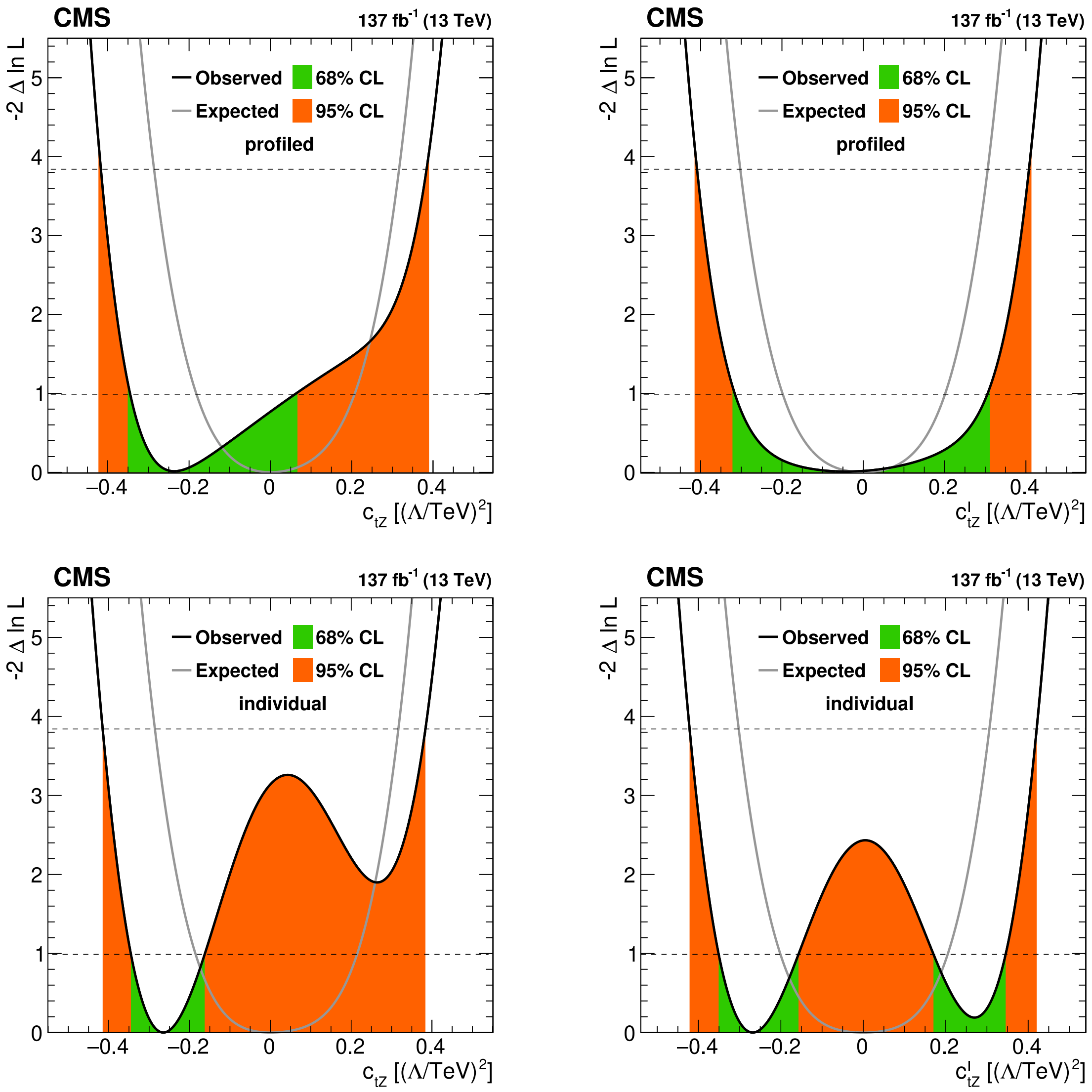

Figure 11: Results of the one-dimensional scans of the Wilson coefficients $c_{\mathrm{tZ}}$ (left) and $c^{\mathrm{I}}_{\mathrm{tZ}}$ (right). In the upper row, the other Wilson coefficient is profiled, while in the lower row it is set to zero. The green and orange bands indicate the 68 and 95% CL contours on the Wilson coefficients, respectively.

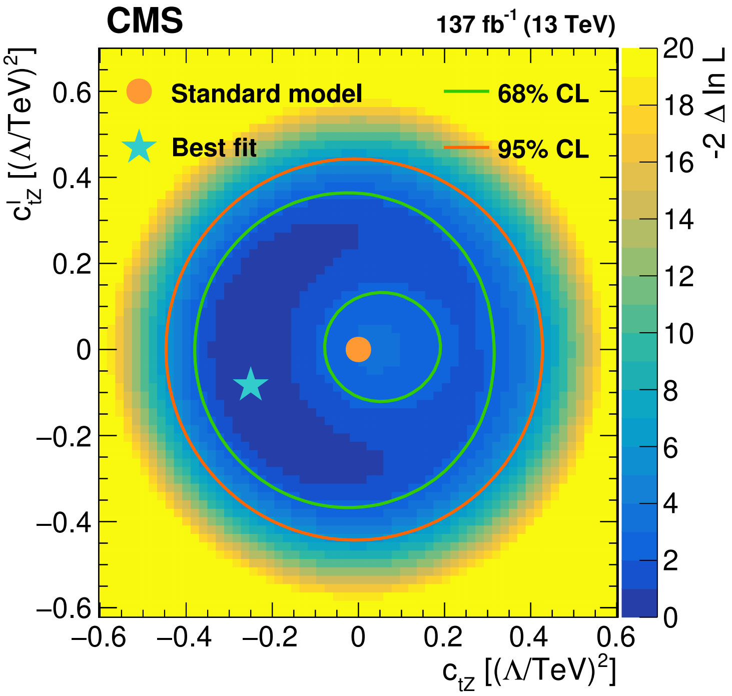

Figure 12: Result of the two-dimensional scan of the Wilson coefficients $c_{tZ}$ and $c^{I}_{tZ}$. The shading quantified by the color scale on the right reflects the negative log-likelihood ratio with respect to the best fit value that is designated by the star. The green and orange lines indicate the 68 and 95% CL contours from the fit, respectively. The allowed areas are those between the two green contours and that inside the orange contour. The dot shows the SM prediction.

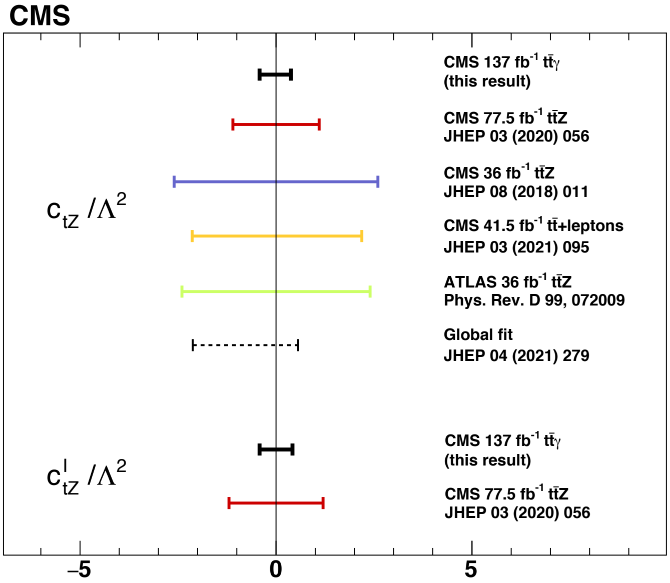

Figure 13: The observed 95% CL intervals for the Wilson coefficients from this measurement with the other Wilson coefficient set to zero, the previous CMS results based on the inclusive [97] and differential [95] $t\bar{t}Z$ cross section measurement, a CMS result based on $t\bar{t}$ in final states with additional leptons [94], and the most recent ATLAS result [96]. The result of a global SM-EFT analysis, including results from Ref. [95], is also shown [98]. The vertical line displays the SM prediction.

## Acknowledgments

We congratulate our colleagues in the CERN accelerator departments for the excellent performance of the LHC and thank the technical and administrative staffs at CERN and at other CMS institutes for their contributions to the success of the CMS effort. In addition, we gratefully acknowledge the computing centers and personnel of the Worldwide LHC Computing Grid and other centers for delivering so effectively the computing infrastructure essential to our analyses. Finally, we acknowledge the enduring support for the construction and operation of the LHC, the CMS detector, and the supporting computing infrastructure provided by the following funding agencies: BMBWF and FWF (Austria); FNRS and FWO (Belgium); CNPq, CAPES, FAPERJ, FAPERGS, and FAPESP (Brazil); MES (Bulgaria); CERN; CAS, MoST, and NSFC (China); MINCIENCIAS (Colombia); MSES and CSF (Croatia); RIF (Cyprus); SENESCYT (Ecuador); MoER, ERC PUT and ERDF (Estonia); Academy of Finland, MEC, and HIP (Finland); CEA and CNRS/IN2P3 (France); BMBF, DFG, and HGF (Germany); GSRT (Greece); NKFIA (Hungary); DAE and DST (India); IPM (Iran); SFI (Ireland); INFN (Italy); MSIP and NRF (Republic of Korea); MES (Latvia); LAS (Lithuania); MOE and UM (Malaysia); BUAP, CINVESTAV, CONACYT, LNS, SEP, and UASLP-FAI (Mexico); MOS (Montenegro); MBIE (New Zealand); PAEC (Pakistan); MSHE and NSC (Poland); FCT (Portugal); JINR (Dubna); MON, RosAtom, RAS, RFBR, and NRC KI (Russia); MESTD (Serbia); SEIDI, CPAN, PCTI, and FEDER (Spain); MOSTR (Sri Lanka); Swiss Funding Agencies (Switzerland); MST (Taipei); ThEPCenter, IPST, STAR, and NSTDA (Thailand); TUBITAK and TAEK (Turkey); NASU (Ukraine); STFC (United Kingdom); DOE and NSF (USA).

Individuals have received support from the Marie-Curie program and the European Research Council and Horizon 2020 Grant, contract Nos. 675440, 724704, 752730, 765710 and 824093 (European Union); the Leventis Foundation; the Alfred P. Sloan Foundation; the Alexander von Humboldt Foundation; the Belgian Federal Science Policy Office; the Fonds pour la Formation à la Recherche dans l'Industrie et dans l'Agriculture (FRIA-Belgium); the Agentschap voor Innovatie door Wetenschap en Technologie (IWT-Belgium); the F.R.S.-FNRS and FWO (Belgium) under the "Excellence of Science – EOS" – be.h project n. 30820817; the Beijing Municipal Science & Technology Commission, No. Z191100007219010; the Ministry of Education, Youth and Sports (MEYS) of the Czech Republic; the Deutsche Forschungsgemeinschaft (DFG), under Germany's Excellence Strategy – EXC 2121 "Quantum Universe" – 390833306, and under project number 400140256 - GRK2497; the Lendület ("Momentum") Program and the János Bolyai Research Scholarship of the Hungarian Academy of Sciences, the New National Excellence Program ÚNKP, the NKFIA research grants 123842, 123959, 124845, 124850, 125105, 128713, 128786, and 129058 (Hungary); the Council of Science and Industrial Research, India; the Latvian Council of Science; the Ministry of Science and Higher Education and the National Science Center, contracts Opus 2014/15/B/ST2/03998 and 2015/19/B/ST2/02861 (Poland); the National Priorities Research Program by Qatar National Research Fund; the Ministry of Science and Higher Education, project no. 0723-2020-0041 (Russia); the Programa Estatal de Fomento de la Investigación Científica y Técnica de Excelencia María de Maeztu, grant MDM-2015-0509 and the Programa Severo Ochoa del Principado de Asturias; the Thalis and Aristeia programs cofinanced by EU-ESF and the Greek NSRF; the Rachadapisek Sompot Fund for Postdoctoral Fellowship, Chulalongkorn University and the Chulalongkorn Academic into Its 2nd Century Project Advancement Project (Thailand); the Kavli Foundation; the Nvidia Corporation; the SuperMicro Corporation; the Welch Foundation, contract C-1845; and the Weston Havens Foundation (USA).

## References

[1] U. Baur, A. Juste, L. H. Orr, and D. Rainwater, "Probing electroweak top quark couplings at hadron colliders", *Phys. Rev. D* **71** (2005) 054013, `doi:10.1103/PhysRevD.71.054013`, `arXiv:hep-ph/0412021`.

[2] A. O. Bouzas and F. Larios, "Electromagnetic dipole moments of the top quark", *Phys. Rev. D* **87** (2013) 074015, `doi:10.1103/PhysRevD.87.074015`, `arXiv:1212.6575`.

[3] M. Schulze and Y. Soreq, "Pinning down electroweak dipole operators of the top quark", *Eur. Phys. J. C* **76** (2016) 466, `doi:10.1140/epjc/s10052-016-4263-x`, `arXiv:1603.08911`.

[4] R. Röntsch and M. Schulze, "Probing top-Z dipole moments at the LHC and ILC", *JHEP* **08** (2015) 044, `doi:10.1007/JHEP08(2015)044`, `arXiv:1501.05939`.

[5] CDF Collaboration, "Evidence for $\mathrm{t\bar{t}}\gamma$ production and measurement of $\sigma_{\mathrm{t\bar{t}}\gamma}/\sigma_{\mathrm{t\bar{t}}}$", *Phys. Rev. D* **48** (2011) 031104, `doi:10.1103/PhysRevD.84.031104`, `arXiv:1106.3970`.

[6] ATLAS Collaboration, "Observation of top-quark pair production in association with a photon and measurement of the $\mathrm{t\bar{t}}\gamma$ production cross section in pp collisions at $\sqrt{s} = 7$ TeV using the ATLAS detector", *Phys. Rev. D* **91** (2015) 072007, `doi:10.1103/PhysRevD.91.072007`, `arXiv:1502.00586`.

[7] ATLAS Collaboration, "Measurement of the $\mathrm{t\bar{t}}\gamma$ production cross section in proton-proton collisions at $\sqrt{s} = 8$ TeV with the ATLAS detector", *JHEP* **11** (2017) 086, `doi:10.1007/JHEP11(2017)086`, `arXiv:1706.03046`.

[8] CMS Collaboration, "Measurement of the semileptonic $\mathrm{t\bar{t}}+\gamma$ production cross section in pp collisions at $\sqrt{s} = 8$ TeV", *JHEP* **10** (2017) 006, `doi:10.1007/JHEP10(2017)006`, `arXiv:1706.08128`.

[9] ATLAS Collaboration, "Measurements of inclusive and differential fiducial cross-sections of $\mathrm{t\bar{t}}\gamma$ production in leptonic final states at $\sqrt{s} = 13$ TeV in ATLAS", *Eur. Phys. J. C* **79** (2019) 382, `doi:10.1140/epjc/s10052-019-6849-6`, `arXiv:1812.01697`.

[10] ATLAS Collaboration, "Measurements of inclusive and differential cross-sections of combined $\mathrm{t\bar{t}}\gamma$ and $\mathrm{tW}\gamma$ production in the $\mathrm{e}\mu$ channel at 13 TeV with the ATLAS detector", *JHEP* **09** (2020) 049, `doi:10.1007/JHEP09(2020)049`, `arXiv:2007.06946`.

[11] O. Bessidskaia Bylund et al., "Probing top quark neutral couplings in the standard model effective field theory at NLO in QCD", *JHEP* **05** (2016) 052, `doi:10.1007/JHEP05(2016)052`, `arXiv:1601.08193`.

[12] D. Barducci et al., "Interpreting top-quark LHC measurements in the standard-model effective field theory", 2018. `arXiv:1802.07237`.

[13] "HEPData record for this analysis", 2021. `doi:10.17182/hepdata.102876`.

[14] CMS Collaboration, "The CMS trigger system", *JINST* **12** (2017) P01020, `doi:10.1088/1748-0221/12/01/P01020`, `arXiv:1609.02366`.

[15] CMS Collaboration, "Performance of the CMS Level-1 trigger in proton-proton collisions at $\sqrt{s} = 13$ TeV", *JINST* **15** (2020) P10017, `doi:10.1088/1748-0221/15/10/P10017`, `arXiv:2006.10165`.

[16] CMS Collaboration, "The CMS experiment at the CERN LHC", *JINST* **3** (2008) S08004, `doi:10.1088/1748-0221/3/08/S08004`.

[17] P. Nason, "A new method for combining NLO QCD with shower Monte Carlo algorithms", *JHEP* **11** (2004) 040, `doi:10.1088/1126-6708/2004/11/040`, `arXiv:hep-ph/0409146`.

[18] S. Frixione, P. Nason, and C. Oleari, "Matching NLO QCD computations with parton shower simulations: the POWHEG method", *JHEP* **11** (2007) 070, `doi:10.1088/1126-6708/2007/11/070`, `arXiv:0709.2092`.

[19] S. Alioli, P. Nason, C. Oleari, and E. Re, "A general framework for implementing NLO calculations in shower Monte Carlo programs: the POWHEG BOX", *JHEP* **06** (2010) 043, `doi:10.1007/JHEP06(2010)043`, `arXiv:1002.2581`.

[20] J. M. Campbell, R. K. Ellis, P. Nason, and E. Re, "Top-pair production and decay at NLO matched with parton showers", *JHEP* **04** (2015) 114, `doi:10.1007/JHEP04(2015)114`, `arXiv:1412.1828`.

[21] S. Alioli, P. Nason, C. Oleari, and E. Re, "NLO single-top production matched with shower in POWHEG: $s$- and $t$-channel contributions", *JHEP* **09** (2009) 111, `doi:10.1088/1126-6708/2009/09/111`, `arXiv:0907.4076`. [Erratum: `doi:10.1007/JHEP02(2010)011`].

[22] S. Frixione, P. Nason, and G. Ridolfi, "A positive-weight next-to-leading-order Monte Carlo for heavy flavour hadroproduction", *JHEP* **09** (2007) 126, `doi:10.1088/1126-6708/2007/09/126`, `arXiv:0707.3088`.

[23] E. Re, "Single-top Wt-channel production matched with parton showers using the POWHEG method", *Eur. Phys. J. C* **71** (2011) 1547, `doi:10.1140/epjc/s10052-011-1547-z`, `arXiv:1009.2450`.

[24] T. Sjöstrand et al., "An introduction to PYTHIA 8.2", *Comput. Phys. Commun.* **191** (2015) 159, `doi:10.1016/j.cpc.2015.01.024`, `arXiv:1410.3012`.

[25] J. Alwall et al., "The automated computation of tree-level and next-to-leading order differential cross sections, and their matching to parton shower simulations", *JHEP* **07** (2014) 079, `doi:10.1007/JHEP07(2014)079`, `arXiv:1405.0301`.

[26] M. Czakon and A. Mitov, "Top++: a program for the calculation of the top-pair cross-section at hadron colliders", *Comput. Phys. Commun.* **185** (2014) 2930, `doi:10.1016/j.cpc.2014.06.021`, `arXiv:1112.5675`.

[27] M. Beneke, P. Falgari, S. Klein, and C. Schwinn, "Hadronic top-quark pair production with NNLL threshold resummation", *Nucl. Phys. B* **855** (2012) 695, `doi:10.1016/j.nuclphysb.2011.10.021`, `arXiv:1109.1536`.

[28] M. Cacciari et al., "Top-pair production at hadron colliders with next-to-next-to-leading logarithmic soft-gluon resummation", *Phys. Lett. B* **710** (2012) 612, `doi:10.1016/j.physletb.2012.03.013`, `arXiv:1111.5869`.

[29] P. Bärnreuther, M. Czakon, and A. Mitov, "Percent level precision physics at the Tevatron: First genuine NNLO QCD corrections to $\mathrm{q\overline{q}} \to \mathrm{t\overline{t}}+X$", *Phys. Rev. Lett.* **109** (2012) 132001, `doi:10.1103/PhysRevLett.109.132001`, `arXiv:1204.5201`.

[30] M. Czakon and A. Mitov, "NNLO corrections to top-pair production at hadron colliders: the all-fermionic scattering channels", *JHEP* **12** (2012) 054, `doi:10.1007/JHEP12(2012)054`, `arXiv:1207.0236`.

[31] M. Czakon and A. Mitov, "NNLO corrections to top pair production at hadron colliders: the quark-gluon reaction", *JHEP* **01** (2013) 080, `doi:10.1007/JHEP01(2013)080`, `arXiv:1210.6832`.

[32] M. Czakon, P. Fiedler, and A. Mitov, "Total top-quark pair-production cross section at hadron colliders through $O(\alpha_S^4)$", *Phys. Rev. Lett.* **110** (2013) 252004, `doi:10.1103/PhysRevLett.110.252004`, `arXiv:1303.6254`.

[33] M. Aliev et al., "HATHOR: HAdronic Top and Heavy quarks crOss section calculatoR", *Comput. Phys. Commun.* **182** (2011) 1034, `doi:10.1016/j.cpc.2010.12.040`, `arXiv:1007.1327`.

[34] P. Kant et al., "HATHOR for single top-quark production: Updated predictions and uncertainty estimates for single top-quark production in hadronic collisions", *Comput. Phys. Commun.* **191** (2015) 74, `doi:10.1016/j.cpc.2015.02.001`, `arXiv:1406.4403`.

[35] N. Kidonakis, "Theoretical results for electroweak-boson and single-top production", *PoS* **DIS2015** (2015) 170, `doi:10.22323/1.247.0170`, `arXiv:1506.04072`.

[36] K. Melnikov and F. Petriello, "Electroweak gauge boson production at hadron colliders through $O(\alpha_S^2)$", *Phys. Rev. D* **74** (2006) 114017, `doi:10.1103/PhysRevD.74.114017`, `arXiv:hep-ph/0609070`.

[37] S. Catani et al., "Vector boson production at hadron colliders: a fully exclusive QCD calculation at NNLO", *Phys. Rev. Lett.* **103** (2009) 082001, `doi:10.1103/PhysRevLett.103.082001`, `arXiv:0903.2120`.

[38] C. Anastasiou, L. J. Dixon, K. Melnikov, and F. Petriello, "High precision QCD at hadron colliders: Electroweak gauge boson rapidity distributions at NNLO", *Phys. Rev. D* **69** (2004) 094008, `doi:10.1103/PhysRevD.69.094008`, `arXiv:hep-ph/0312266`.

[39] S. Dittmaier, A. Huss, and C. Schwinn, "Mixed QCD-electroweak $O(\alpha_S\alpha)$ corrections to Drell–Yan processes in the resonance region: pole approximation and non-factorizable corrections", *Nucl. Phys. B* **885** (2014) 318, `doi:10.1016/j.nuclphysb.2014.05.027`, `arXiv:1403.3216`.

[40] J. M. Lindert et al., "Precise predictions for V+jets dark matter backgrounds", *Eur. Phys. J. C* **77** (2017) 829, `doi:10.1140/epjc/s10052-017-5389-1`, `arXiv:1705.04664`.

[41] M. V. Garzelli, A. Kardos, C. G. Papadopoulos, and Z. Trocsanyi, "$\mathrm{t\bar{t}W^{\pm}}$ and $\mathrm{t\bar{t}Z}$ hadroproduction at NLO accuracy in QCD with parton shower and hadronization effects", *JHEP* **11** (2012) 056, `doi:10.1007/JHEP11(2012)056`, `arXiv:1208.2665`.

[42] S. Frixione et al., "Electroweak and QCD corrections to top-pair hadroproduction in association with heavy bosons", *JHEP* **06** (2015) 184, `doi:10.1007/JHEP06(2015)184`, `arXiv:1504.03446`.

[43] T. Gehrmann et al., "$\mathrm{W^+W^-}$ production at hadron colliders in next to next to leading order QCD", *Phys. Rev. Lett.* **113** (2014) 212001, `doi:10.1103/PhysRevLett.113.212001`, `arXiv:1408.5243`.

[44] P. Skands, S. Carrazza, and J. Rojo, "Tuning PYTHIA 8.1: the Monash 2013 tune", *Eur. Phys. J. C* **74** (2014) 3024, `doi:10.1140/epjc/s10052-014-3024-y`, `arXiv:1404.5630`.

[45] CMS Collaboration, "Event generator tunes obtained from underlying event and multiparton scattering measurements", *Eur. Phys. J. C* **76** (2016) 155, `doi:10.1140/epjc/s10052-016-3988-x`, `arXiv:1512.00815`.

[46] CMS Collaboration, "Extraction and validation of a new set of CMS PYTHIA8 tunes from underlying-event measurements", *Eur. Phys. J. C* **80** (2020) 4, `doi:10.1140/epjc/s10052-019-7499-4`, `arXiv:1903.12179`.

[47] NNPDF Collaboration, "Parton distributions from high-precision collider data", *Eur. Phys. J. C* **77** (2017) 663, `doi:10.1140/epjc/s10052-017-5199-5`, `arXiv:1706.00428`.

[48] NNPDF Collaboration, "Parton distributions for the LHC Run II", *JHEP* **04** (2015) 040, `doi:10.1007/JHEP04(2015)040`, `arXiv:1410.8849`.

[49] J. Alwall et al., "Comparative study of various algorithms for the merging of parton showers and matrix elements in hadronic collisions", *Eur. Phys. J. C* **53** (2008) 473, `doi:10.1140/epjc/s10052-007-0490-5`, `arXiv:0706.2569`.

[50] R. Frederix and S. Frixione, "Merging meets matching in MC@NLO", *JHEP* **12** (2012) 061, `doi:10.1007/JHEP12(2012)061`, `arXiv:1209.6215`.

[51] GEANT4 Collaboration, "GEANT4—a simulation toolkit", *Nucl. Instrum. Meth. A* **506** (2003) 250, `doi:10.1016/S0168-9002(03)01368-8`.

[52] CMS Collaboration, "Measurement of the inelastic proton-proton cross section at $\sqrt{s} = 13$ TeV", *JHEP* **07** (2018) 161, `doi:10.1007/JHEP07(2018)161`, `arXiv:1802.02613`.

[53] CMS Collaboration, "Particle-flow reconstruction and global event description with the CMS detector", *JINST* **12** (2017) P10003, `doi:10.1088/1748-0221/12/10/P10003`, `arXiv:1706.04965`.

[54] CMS Collaboration, "Performance of the CMS muon detector and muon reconstruction with proton-proton collisions at $\sqrt{s} = 13$ TeV", *JINST* **13** (2018) P06015, `doi:10.1088/1748-0221/13/06/P06015`, `arXiv:1804.04528`.

[55] CMS Collaboration, "Performance of electron reconstruction and selection with the CMS detector in proton-proton collisions at $\sqrt{s} = 8$ TeV", *JINST* **10** (2015) P06005, `doi:10.1088/1748-0221/10/06/P06005`, `arXiv:1502.02701`.

[56] CMS Collaboration, "Performance of photon reconstruction and identification with the CMS detector in proton-proton collisions at $\sqrt{s} = 8$ TeV", *JINST* **10** (2015) P08010, `doi:10.1088/1748-0221/10/08/P08010`, `arXiv:1502.02702`.

[57] CMS Collaboration, "Electron and photon reconstruction and identification with the CMS experiment at the CERN LHC", *JINST* **16** (2021) P05014, `doi:10.1088/1748-0221/16/05/P05014`, `arXiv:2012.06888`.

[58] CMS Collaboration, "Performance of CMS muon reconstruction in pp collision events at $\sqrt{s} = 7$ TeV", *JINST* **7** (2012) P10002, `doi:10.1088/1748-0221/7/10/P10002`, `arXiv:1206.4071`.

[59] M. Cacciari, G. P. Salam, and G. Soyez, "The anti-$k_{\mathrm{T}}$ jet clustering algorithm", *JHEP* **04** (2008) 063, `doi:10.1088/1126-6708/2008/04/063`, `arXiv:0802.1189`.

[60] M. Cacciari, G. P. Salam, and G. Soyez, "FastJet user manual", *Eur. Phys. J. C* **72** (2012) 1896, `doi:10.1140/epjc/s10052-012-1896-2`, `arXiv:1111.6097`.

[61] CMS Collaboration, "Jet energy scale and resolution in the CMS experiment in pp collisions at 8 TeV", *JINST* **12** (2017) P02014, `doi:10.1088/1748-0221/12/02/P02014`, `arXiv:1607.03663`.

[62] CMS Collaboration, "Identification of heavy-flavour jets with the CMS detector in pp collisions at 13 TeV", *JINST* **13** (2018) P05011, `doi:10.1088/1748-0221/13/05/P05011`, `arXiv:1712.07158`.

[63] CMS Collaboration, "Measurement of the differential Drell–Yan cross section in proton-proton collisions at $\sqrt{s} = 13$ TeV", *JHEP* **12** (2019) 059, `doi:10.1007/JHEP12(2019)059`, `arXiv:1812.10529`.

[64] M. Cacciari and G. P. Salam, "Pileup subtraction using jet areas", *Phys. Lett. B* **659** (2008) 119, `doi:10.1016/j.physletb.2007.09.077`, `arXiv:0707.1378`.

[65] CMS Collaboration, "Measurement of the top-antitop production cross section in pp collisions at $\sqrt{s} = 7$ TeV using the kinematic properties of events with leptons and jets", *Eur. Phys. J. C* **71** (2011) 1721, `doi:10.1140/epjc/s10052-011-1721-3`, `arXiv:1106.0902`.

[66] Particle Data Group, P. A. Zyla et al., "Review of particle physics", *Prog. Theor. Exp. Phys.* **2020** (2020) 083C01, `doi:10.1093/ptep/ptaa104`.

[67] The ATLAS Collaboration, The CMS Collaboration, The LHC Higgs Combination Group, "Procedure for the LHC Higgs boson search combination in Summer 2011", Technical Report CMS-NOTE-2011-005, ATL-PHYS-PUB-2011-11, 2011.

[68] G. Cowan, K. Cranmer, E. Gross, and O. Vitells, "Asymptotic formulae for likelihood-based tests of new physics", *Eur. Phys. J. C* **71** (2011) 1554, `doi:10.1140/epjc/s10052-011-1554-0`, `arXiv:1007.1727`. [Erratum: `doi:10.1140/epjc/s10052-013-2501-z`].

[69] CMS Collaboration, "Precision luminosity measurement in proton-proton collisions at $\sqrt{s} = 13$ TeV in 2015 and 2016 at CMS", 2021. `arXiv:2104.01927`. Submitted to EPJC.

[70] CMS Collaboration, "CMS luminosity measurement for the 2017 data-taking period at $\sqrt{s} = 13$ TeV", Technical Report CMS-PAS-LUM-17-004, 2018.

[71] CMS Collaboration, "CMS luminosity measurement for the 2018 data-taking period at $\sqrt{s} = 13$ TeV", Technical Report CMS-PAS-LUM-18-002, 2019.

[72] ATLAS Collaboration, "Measurement of the inelastic proton-proton cross section at $\sqrt{s} = 13$ TeV with the ATLAS detector at the LHC", *Phys. Rev. Lett.* **117** (2016) 182002, `doi:10.1103/PhysRevLett.117.182002`, `arXiv:1606.02625`.

[73] CMS Collaboration, “Energy calibration and resolution of the CMS electromagnetic calorimeter in pp collisions at $\sqrt{s} = 7$ TeV”, *JINST* **8** (2013) P09009, `doi:10.1088/1748-0221/8/09/P09009`, `arXiv:1306.2016`.

[74] CMS Collaboration, “Identification of b-quark jets with the CMS experiment”, *JINST* **8** (2013) P04013, `doi:10.1088/1748-0221/8/04/P04013`, `arXiv:1211.4462`.

[75] S. Argyropoulos and T. Sjöstrand, “Effects of color reconnection on $t\bar{t}$ final states at the LHC”, *JHEP* **11** (2014) 043, `doi:10.1007/JHEP11(2014)043`, `arXiv:1407.6653`.

[76] J. R. Christiansen and P. Z. Skands, “String formation beyond leading colour”, *JHEP* **08** (2015) 003, `doi:10.1007/JHEP08(2015)003`, `arXiv:1505.01681`.

[77] G. Cowan, “Statistical data analysis”. Clarendon Press, 1998.

[78] S. Schmitt, “TUnfold, an algorithm for correcting migration effects in high energy physics”, *JINST* **7** (2012) T10003, `doi:10.1088/1748-0221/7/10/T10003`, `arXiv:1205.6201`.

[79] J. Bellm et al., “Herwig 7.0/Herwig++ 3.0 release note”, *Eur. Phys. J. C* **76** (2016) 196, `doi:10.1140/epjc/s10052-016-4018-8`, `arXiv:1512.01178`.

[80] CMS Collaboration, “Development and validation of HERWIG 7 tunes from CMS underlying-event measurements”, *Eur. Phys. J. C* **81** (2021) 312, `doi:10.1140/epjc/s10052-021-08949-5`, `arXiv:2011.03422`.

[81] W. Hollik et al., “Top dipole form-factors and loop induced CP violation in supersymmetry”, *Nucl. Phys. B* **551** (1999) 3, `doi:10.1016/S0550-3213(99)00201-1`, `arXiv:hep-ph/9812298`. [Erratum: `doi:10.1016/S0550-3213(99)00396-X`].

[82] K. Agashe, G. Perez, and A. Soni, “Collider signals of top quark flavor violation from a warped extra dimension”, *Phys. Rev. D* **75** (2007) 015002, `doi:10.1103/PhysRevD.75.015002`, `arXiv:hep-ph/0606293`.

[83] A. L. Kagan, G. Perez, T. Volansky, and J. Zupan, “General minimal flavor violation”, *Phys. Rev. D* **80** (2009) 076002, `doi:10.1103/PhysRevD.80.076002`, `arXiv:0903.1794`.

[84] T. Ibrahim and P. Nath, “The top quark electric dipole moment in an MSSM extension with vector like multiplets”, *Phys. Rev. D* **82** (2010) 055001, `doi:10.1103/PhysRevD.82.055001`, `arXiv:1007.0432`.

[85] T. Ibrahim and P. Nath, “The chromoelectric dipole moment of the top quark in models with vector like multiplets”, *Phys. Rev. D* **84** (2011) 015003, `doi:10.1103/PhysRevD.84.015003`, `arXiv:1104.3851`.

[86] C. Grojean, O. Matsedonskyi, and G. Panico, “Light top partners and precision physics”, *JHEP* **10** (2013) 160, `doi:10.1007/JHEP10(2013)160`, `arXiv:1306.4655`.

[87] F. Richard, “Can LHC observe an anomaly in ttZ production?”, 2013. `arXiv:1304.3594`.

[88] B. Grzadkowski, M. Iskrzynski, M. Misiak, and J. Rosiek, “Dimension-six terms in the standard model Lagrangian”, *JHEP* **10** (2010) 085, `doi:10.1007/JHEP10(2010)085`, `arXiv:1008.4884`.

[89] C. Zhang and S. Willenbrock, "Effective-field-theory approach to top-quark production and decay", *Phys. Rev. D* **83** (2011) 034006, `doi:10.1103/PhysRevD.83.034006`, `arXiv:1008.3869`.

[90] CMS Collaboration, "Measurements of $\mathrm{t\bar{t}}$ differential cross sections in proton-proton collisions at $\sqrt{s} = 13$ TeV using events containing two leptons", *JHEP* **02** (2019) 149, `doi:10.1007/JHEP02(2019)149`, `arXiv:1811.06625`.

[91] CMS Collaboration, "Measurement of the top quark polarization and $\mathrm{t\bar{t}}$ spin correlations using dilepton final states in proton-proton collisions at $\sqrt{s} = 13$ TeV", *Phys. Rev. D* **100** (2019) 072002, `doi:10.1103/PhysRevD.100.072002`, `arXiv:1907.03729`.

[92] CMS Collaboration, "Measurement of the W boson helicity fractions in the decays of top quark pairs to lepton+jets final states produced in pp collisions at $\sqrt{s} = 8$ TeV", *Phys. Lett. B* **762** (2016) 512, `doi:10.1016/j.physletb.2016.10.007`, `arXiv:1605.09047`.

[93] J. A. Aguilar-Saavedra and J. Bernabeu, "W polarisation beyond helicity fractions in top quark decays", *Nucl. Phys. B* **840** (2010) 349, `doi:10.1016/j.nuclphysb.2010.07.012`, `arXiv:1005.5382`.

[94] CMS Collaboration, "Search for new physics in top quark production with additional leptons in proton-proton collisions at $\sqrt{s} = 13$ TeV using effective field theory", *JHEP* **03** (2021) 095, `doi:10.1007/JHEP03(2021)095`, `arXiv:2012.04120`.

[95] CMS Collaboration, "Measurement of top quark pair production in association with a Z boson in proton-proton collisions at $\sqrt{s} = 13$ TeV", *JHEP* **03** (2020) 056, `doi:10.1007/JHEP03(2020)056`, `arXiv:1907.11270`.

[96] ATLAS Collaboration, "Measurement of the $\mathrm{t\bar{t}Z}$ and $\mathrm{t\bar{t}W}$ cross sections in proton-proton collisions at $\sqrt{s} = 13$ TeV with the ATLAS detector", *Phys. Rev. D* **99** (2019) 072009, `doi:10.1103/PhysRevD.99.072009`, `arXiv:1901.03584`.

[97] CMS Collaboration, "Measurement of the cross section for top quark pair production in association with a W or Z boson in proton-proton collisions at $\sqrt{s} = 13$ TeV", *JHEP* **08** (2018) 011, `doi:10.1007/JHEP08(2018)011`, `arXiv:1711.02547`.

[98] J. Ellis et al., "Top, Higgs, diboson and electroweak fit to the standard model effective field theory", *JHEP* **04** (2021) 279, `doi:10.1007/JHEP04(2021)279`, `arXiv:2012.02779`.

## A The CMS Collaboration

**Yerevan Physics Institute, Yerevan, Armenia**
A. Tumasyan

**Institut für Hochenergiephysik, Wien, Austria**
W. Adam, J.W. Andrejkovic, T. Bergauer, S. Chatterjee, M. Dragicevic, A. Escalante Del Valle, R. Frühwirth[1], M. Jeitler[1], N. Krammer, L. Lechner, D. Liko, I. Mikulec, P. Paulitsch, F.M. Pitters, J. Schieck[1], R. Schöfbeck, M. Spanring, S. Templ, W. Waltenberger, C.-E. Wulz[1]

**Institute for Nuclear Problems, Minsk, Belarus**
V. Chekhovsky, A. Litomin, V. Makarenko

**Universiteit Antwerpen, Antwerpen, Belgium**
M.R. Darwish[2], E.A. De Wolf, X. Janssen, T. Kello[3], A. Lelek, H. Rejeb Sfar, P. Van Mechelen, S. Van Putte, N. Van Remortel

**Vrije Universiteit Brussel, Brussel, Belgium**
F. Blekman, E.S. Bols, J. D’Hondt, J. De Clercq, M. Delcourt, H. El Faham, S. Lowette, S. Moortgat, A. Morton, D. Müller, A.R. Sahasransu, S. Tavernier, W. Van Doninck, P. Van Mulders

**Université Libre de Bruxelles, Bruxelles, Belgium**
D. Beghin, B. Bilin, B. Clerbaux, G. De Lentdecker, L. Favart, A. Grebenyuk, A.K. Kalsi, K. Lee, M. Mahdavikhorrami, I. Makarenko, L. Moureaux, L. Pétré, A. Popov, N. Postiau, E. Starling, L. Thomas, M. Vanden Bemden, C. Vander Velde, P. Vanlaer, D. Vannerom, L. Wezenbeek

**Ghent University, Ghent, Belgium**
T. Cornelis, D. Dobur, J. Knolle, L. Lambrecht, G. Mestdach, M. Niedziela, C. Roskas, A. Samalan, K. Skovpen, M. Tytgat, W. Verbeke, B. Vermassen, M. Vit

**Université Catholique de Louvain, Louvain-la-Neuve, Belgium**
A. Bethani, G. Bruno, F. Bury, C. Caputo, P. David, C. Delaere, I.S. Donertas, A. Giammanco, K. Jaffel, Sa. Jain, V. Lemaitre, K. Mondal, J. Prisciandaro, A. Taliercio, M. Teklishyn, T.T. Tran, P. Vischia, S. Wertz

**Centro Brasileiro de Pesquisas Fisicas, Rio de Janeiro, Brazil**
G.A. Alves, C. Hensel, A. Moraes

**Universidade do Estado do Rio de Janeiro, Rio de Janeiro, Brazil**
W.L. Aldá Júnior, M. Alves Gallo Pereira, M. Barroso Ferreira Filho, H. BRANDAO MALBOUISSON, W. Carvalho, J. Chinellato[4], E.M. Da Costa, G.G. Da Silveira[5], D. De Jesus Damiao, S. Fonseca De Souza, D. Matos Figueiredo, C. Mora Herrera, K. Mota Amarilo, L. Mundim, H. Nogima, P. Rebello Teles, A. Santoro, S.M. Silva Do Amaral, A. Sznajder, M. Thiel, F. Torres Da Silva De Araujo, A. Vilela Pereira

**Universidade Estadual Paulista [a], Universidade Federal do ABC [b], São Paulo, Brazil**
C.A. Bernardes[a,a,5], L. Calligaris[a], T.R. Fernandez Perez Tomei[a], E.M. Gregores[a,b], D.S. Lemos[a], P.G. Mercadante[a,b], S.F. Novaes[a], Sandra S. Padula[a]

**Institute for Nuclear Research and Nuclear Energy, Bulgarian Academy of Sciences, Sofia, Bulgaria**
A. Aleksandrov, G. Antchev, R. Hadjiiska, P. Iaydjiev, M. Misheva, M. Rodozov, M. Shopova, G. Sultanov

**University of Sofia, Sofia, Bulgaria**
A. Dimitrov, T. Ivanov, L. Litov, B. Pavlov, P. Petkov, A. Petrov

**Beihang University, Beijing, China**
T. Cheng, Q. Guo, T. Javaid[6], M. Mittal, H. Wang, L. Yuan

**Department of Physics, Tsinghua University, Beijing, China**
M. Ahmad, G. Bauer, C. Dozen[7], Z. Hu, J. Martins[8], Y. Wang, K. Yi[9,10]

**Institute of High Energy Physics, Beijing, China**
E. Chapon, G.M. Chen[6], H.S. Chen[6], M. Chen, F. Iemmi, A. Kapoor, D. Leggat, H. Liao, Z.-A. LIU[6], V. Milosevic, F. Monti, R. Sharma, J. Tao, J. Thomas-wilsker, J. Wang, H. Zhang, S. Zhang[6], J. Zhao

**State Key Laboratory of Nuclear Physics and Technology, Peking University, Beijing, China**
A. Agapitos, Y. Ban, C. Chen, Q. Huang, A. Levin, Q. Li, X. Lyu, Y. Mao, S.J. Qian, D. Wang, Q. Wang, J. Xiao

**Sun Yat-Sen University, Guangzhou, China**
M. Lu, Z. You

**Institute of Modern Physics and Key Laboratory of Nuclear Physics and Ion-beam Application (MOE) - Fudan University, Shanghai, China**
X. Gao[3], H. Okawa

**Zhejiang University, Hangzhou, China**
Z. Lin, M. Xiao

**Universidad de Los Andes, Bogota, Colombia**
C. Avila, A. Cabrera, C. Florez, J. Fraga, A. Sarkar, M.A. Segura Delgado

**Universidad de Antioquia, Medellin, Colombia**
J. Mejia Guisao, F. Ramirez, J.D. Ruiz Alvarez, C.A. Salazar González

**University of Split, Faculty of Electrical Engineering, Mechanical Engineering and Naval Architecture, Split, Croatia**
D. Giljanovic, N. Godinovic, D. Lelas, I. Puljak

**University of Split, Faculty of Science, Split, Croatia**
Z. Antunovic, M. Kovac, T. Sculac

**Institute Rudjer Boskovic, Zagreb, Croatia**
V. Brigljevic, D. Ferencek, D. Majumder, M. Roguljic, A. Starodumov[11], T. Susa

**University of Cyprus, Nicosia, Cyprus**
A. Attikis, K. Christoforou, E. Erodotou, A. Ioannou, G. Kole, M. Kolosova, S. Konstantinou, J. Mousa, C. Nicolaou, F. Ptochos, P.A. Razis, H. Rykaczewski, H. Saka

**Charles University, Prague, Czech Republic**
M. Finger[12], M. Finger Jr.[12], A. Kveton

**Escuela Politecnica Nacional, Quito, Ecuador**
E. Ayala

**Universidad San Francisco de Quito, Quito, Ecuador**
E. Carrera Jarrin

**Academy of Scientific Research and Technology of the Arab Republic of Egypt, Egyptian Network of High Energy Physics, Cairo, Egypt**
H. Abdalla[13], S. Khalil[14]

**Center for High Energy Physics (CHEP-FU), Fayoum University, El-Fayoum, Egypt**
A. Lotfy, M.A. Mahmoud

**National Institute of Chemical Physics and Biophysics, Tallinn, Estonia**
S. Bhowmik, A. Carvalho Antunes De Oliveira, R.K. Dewanjee, K. Ehataht, M. Kadastik, S. Nandan, C. Nielsen, J. Pata, M. Raidal, L. Tani, C. Veelken

**Department of Physics, University of Helsinki, Helsinki, Finland**
P. Eerola, L. Forthomme, H. Kirschenmann, K. Osterberg, M. Voutilainen

**Helsinki Institute of Physics, Helsinki, Finland**
S. Bharthuar, E. Brücken, F. Garcia, J. Havukainen, M.S. Kim, R. Kinnunen, T. Lampén, K. Lassila-Perini, S. Lehti, T. Lindén, M. Lotti, L. Martikainen, M. Myllymäki, J. Ott, H. Siikonen, E. Tuominen, J. Tuominiemi

**Lappeenranta University of Technology, Lappeenranta, Finland**
P. Luukka, H. Petrow, T. Tuuva

**IRFU, CEA, Université Paris-Saclay, Gif-sur-Yvette, France**
C. Amendola, M. Besancon, F. Couderc, M. Dejardin, D. Denegri, J.L. Faure, F. Ferri, S. Ganjour, A. Givernaud, P. Gras, G. Hamel de Monchenault, P. Jarry, B. Lenzi, E. Locci, J. Malcles, J. Rander, A. Rosowsky, M.Ö. Sahin, A. Savoy-Navarro[15], M. Titov, G.B. Yu

**Laboratoire Leprince-Ringuet, CNRS/IN2P3, Ecole Polytechnique, Institut Polytechnique de Paris, Palaiseau, France**
S. Ahuja, F. Beaudette, M. Bonanomi, A. Buchot Perraguin, P. Busson, A. Cappati, C. Charlot, O. Davignon, B. Diab, G. Falmagne, S. Ghosh, R. Granier de Cassagnac, A. Hakimi, I. Kucher, M. Nguyen, C. Ochando, P. Paganini, J. Rembser, R. Salerno, J.B. Sauvan, Y. Sirois, A. Zabi, A. Zghiche

**Université de Strasbourg, CNRS, IPHC UMR 7178, Strasbourg, France**
J.-L. Agram[16], J. Andrea, D. Apparu, D. Bloch, G. Bourgatte, J.-M. Brom, E.C. Chabert, C. Collard, D. Darej, J.-C. Fontaine[16], U. Goerlach, C. Grimault, A.-C. Le Bihan, E. Nibigira, P. Van Hove

**Institut de Physique des 2 Infinis de Lyon (IP2I ), Villeurbanne, France**
E. Asilar, S. Beauceron, C. Bernet, G. Boudoul, C. Camen, A. Carle, N. Chanon, D. Contardo, P. Depasse, H. El Mamouni, J. Fay, S. Gascon, M. Gouzevitch, B. Ille, I.B. Laktineh, H. Lattaud, A. Lesauvage, M. Lethuillier, L. Mirabito, S. Perries, K. Shchablo, V. Sordini, L. Torterotot, G. Touquet, M. Vander Donckt, S. Viret

**Georgian Technical University, Tbilisi, Georgia**
I. Lomidze, T. Toriashvili[17], Z. Tsamalaidze[12]

**RWTH Aachen University, I. Physikalisches Institut, Aachen, Germany**
L. Feld, K. Klein, M. Lipinski, D. Meuser, A. Pauls, M.P. Rauch, N. Röwert, J. Schulz, M. Teroerde

**RWTH Aachen University, III. Physikalisches Institut A, Aachen, Germany**
A. Dodonova, D. Eliseev, M. Erdmann, P. Fackeldey, B. Fischer, S. Ghosh, T. Hebbeker, K. Hoepfner, F. Ivone, H. Keller, L. Mastrolorenzo, M. Merschmeyer, A. Meyer, G. Mocellin,

S. Mondal, S. Mukherjee, D. Noll, A. Novak, T. Pook, A. Pozdnyakov, Y. Rath, H. Reithler, J. Roemer, A. Schmidt, S.C. Schuler, A. Sharma, L. Vigilante, S. Wiedenbeck, S. Zaleski

**RWTH Aachen University, III. Physikalisches Institut B, Aachen, Germany**
C. Dziwok, G. Flügge, W. Haj Ahmad[18], O. Hlushchenko, T. Kress, A. Nowack, C. Pistone, O. Pooth, D. Roy, H. Sert, A. Stahl[19], T. Ziemons

**Deutsches Elektronen-Synchrotron, Hamburg, Germany**
H. Aarup Petersen, M. Aldaya Martin, P. Asmuss, I. Babounikau, S. Baxter, O. Behnke, A. Bermúdez Martínez, S. Bhattacharya, A.A. Bin Anuar, K. Borras[20], V. Botta, D. Brunner, A. Campbell, A. Cardini, C. Cheng, F. Colombina, S. Consuegra Rodríguez, G. Correia Silva, V. Danilov, L. Didukh, G. Eckerlin, D. Eckstein, L.I. Estevez Banos, O. Filatov, E. Gallo[21], A. Geiser, A. Giraldi, A. Grohsjean, M. Guthoff, A. Jafari[22], N.Z. Jomhari, H. Jung, A. Kasem[20], M. Kasemann, H. Kaveh, C. Kleinwort, D. Krücker, W. Lange, J. Lidrych, K. Lipka, W. Lohmann[23], R. Mankel, I.-A. Melzer-Pellmann, J. Metwally, A.B. Meyer, M. Meyer, J. Mnich, A. Mussgiller, Y. Otarid, D. Pérez Adán, D. Pitzl, A. Raspereza, B. Ribeiro Lopes, J. Rübenach, A. Saggio, A. Saibel, M. Savitskyi, M. Scham, V. Scheurer, C. Schwanenberger[21], A. Singh, R.E. Sosa Ricardo, D. Stafford, N. Tonon, O. Turkot, M. Van De Klundert, R. Walsh, D. Walter, Y. Wen, K. Wichmann, L. Wiens, C. Wissing, S. Wuchterl

**University of Hamburg, Hamburg, Germany**
R. Aggleton, S. Albrecht, S. Bein, L. Benato, A. Benecke, P. Connor, K. De Leo, M. Eich, F. Feindt, A. Fröhlich, C. Garbers, E. Garutti, P. Gunnellini, J. Haller, A. Hinzmann, G. Kasieczka, R. Klanner, R. Kogler, T. Kramer, V. Kutzner, J. Lange, T. Lange, A. Lobanov, A. Malara, A. Nigamova, K.J. Pena Rodriguez, O. Rieger, P. Schleper, M. Schröder, J. Schwandt, D. Schwarz, J. Sonneveld, H. Stadie, G. Steinbrück, A. Tews, B. Vormwald, I. Zoi

**Karlsruher Institut fuer Technologie, Karlsruhe, Germany**
J. Bechtel, T. Berger, E. Butz, R. Caspart, T. Chwalek, W. De Boer†, A. Dierlamm, A. Droll, K. El Morabit, N. Faltermann, M. Giffels, J.o. Gosewisch, A. Gottmann, F. Hartmann[19], C. Heidecker, U. Husemann, I. Katkov[24], P. Keicher, R. Koppenhöfer, S. Maier, M. Metzler, S. Mitra, Th. Müller, M. Neukum, A. Nürnberg, G. Quast, K. Rabbertz, J. Rauser, D. Savoiu, M. Schnepf, D. Seith, I. Shvetsov, H.J. Simonis, R. Ulrich, J. Van Der Linden, R.F. Von Cube, M. Wassmer, M. Weber, S. Wieland, R. Wolf, S. Wozniewski, S. Wunsch

**Institute of Nuclear and Particle Physics (INPP), NCSR Demokritos, Aghia Paraskevi, Greece**
G. Anagnostou, G. Daskalakis, T. Geralis, A. Kyriakis, D. Loukas, A. Stakia

**National and Kapodistrian University of Athens, Athens, Greece**
M. Diamantopoulou, D. Karasavvas, G. Karathanasis, P. Kontaxakis, C.K. Koraka, A. Manousakis-katsikakis, A. Panagiotou, I. Papavergou, N. Saoulidou, K. Theofilatos, E. Tziaferi, K. Vellidis, E. Vourliotis

**National Technical University of Athens, Athens, Greece**
G. Bakas, K. Kousouris, I. Papakrivopoulos, G. Tsipolitis, A. Zacharopoulou

**University of Ioánnina, Ioánnina, Greece**
I. Evangelou, C. Foudas, P. Gianneios, P. Katsoulis, P. Kokkas, N. Manthos, I. Papadopoulos, J. Strologas

**MTA-ELTE Lendület CMS Particle and Nuclear Physics Group, Eötvös Loránd University,**

**Budapest, Hungary**
M. Csanad, K. Farkas, M.M.A. Gadallah[25], S. Lökös[26], P. Major, K. Mandal, A. Mehta, G. Pasztor, A.J. Rádl, O. Surányi, G.I. Veres

**Wigner Research Centre for Physics, Budapest, Hungary**
M. Bartók[27], G. Bencze, C. Hajdu, D. Horvath[28], F. Sikler, V. Veszpremi, G. Vesztergombi[†]

**Institute of Nuclear Research ATOMKI, Debrecen, Hungary**
S. Czellar, J. Karancsi[27], J. Molnar, Z. Szillasi, D. Teyssier

**Institute of Physics, University of Debrecen, Debrecen, Hungary**
P. Raics, Z.L. Trocsanyi[29], B. Ujvari

**Karoly Robert Campus, MATE Institute of Technology**
T. Csorgo[30], F. Nemes[30], T. Novak

**Indian Institute of Science (IISc), Bangalore, India**
J.R. Komaragiri, D. Kumar, L. Panwar, P.C. Tiwari

**National Institute of Science Education and Research, HBNI, Bhubaneswar, India**
S. Bahinipati[31], A.K. Das, C. Kar, P. Mal, T. Mishra, V.K. Muraleedharan Nair Bindhu[32], A. Nayak[32], P. Saha, N. Sur, S.K. Swain, D. Vats[32]

**Panjab University, Chandigarh, India**
S. Bansal, S.B. Beri, V. Bhatnagar, G. Chaudhary, S. Chauhan, N. Dhingra[33], R. Gupta, A. Kaur, M. Kaur, S. Kaur, P. Kumari, M. Meena, K. Sandeep, J.B. Singh, A.K. Virdi

**University of Delhi, Delhi, India**
A. Ahmed, A. Bhardwaj, B.C. Choudhary, M. Gola, S. Keshri, A. Kumar, M. Naimuddin, P. Priyanka, K. Ranjan, A. Shah

**Saha Institute of Nuclear Physics, HBNI, Kolkata, India**
M. Bharti[34], R. Bhattacharya, S. Bhattacharya, D. Bhowmik, S. Dutta, S. Dutta, B. Gomber[35], M. Maity[36], P. Palit, P.K. Rout, G. Saha, B. Sahu, S. Sarkar, M. Sharan, B. Singh[34], S. Thakur[34]

**Indian Institute of Technology Madras, Madras, India**
P.K. Behera, S.C. Behera, P. Kalbhor, A. Muhammad, R. Pradhan, P.R. Pujahari, A. Sharma, A.K. Sikdar

**Bhabha Atomic Research Centre, Mumbai, India**
D. Dutta, V. Jha, V. Kumar, D.K. Mishra, K. Naskar[37], P.K. Netrakanti, L.M. Pant, P. Shukla

**Tata Institute of Fundamental Research-A, Mumbai, India**
T. Aziz, S. Dugad, M. Kumar, U. Sarkar

**Tata Institute of Fundamental Research-B, Mumbai, India**
S. Banerjee, R. Chudasama, M. Guchait, S. Karmakar, S. Kumar, G. Majumder, K. Mazumdar, S. Mukherjee

**Indian Institute of Science Education and Research (IISER), Pune, India**
K. Alpana, S. Dube, B. Kansal, A. Laha, S. Pandey, A. Rane, A. Rastogi, S. Sharma

**Department of Physics, Isfahan University of Technology, Isfahan, Iran**
H. Bakhshiansohi[38], M. Zeinali[39]

**Institute for Research in Fundamental Sciences (IPM), Tehran, Iran**
S. Chenarani[40], S.M. Etesami, M. Khakzad, M. Mohammadi Najafabadi

**University College Dublin, Dublin, Ireland**
M. Grunewald

**INFN Sezione di Bari [a], Università di Bari [b], Politecnico di Bari [c], Bari, Italy**
M. Abbrescia[a,b], R. Aly[a,b,41], C. Aruta[a,b], A. Colaleo[a], D. Creanza[a,c], N. De Filippis[a,c], M. De Palma[a,b], A. Di Florio[a,b], A. Di Pilato[a,b], W. Elmetenawee[a,b], L. Fiore[a], A. Gelmi[a,b], M. Gul[a], G. Iaselli[a,c], M. Ince[a,b], S. Lezki[a,b], G. Maggi[a,c], M. Maggi[a], I. Margjeka[a,b], V. Mastrapasqua[a,b], J.A. Merlin[a], S. My[a,b], S. Nuzzo[a,b], A. Pellecchia[a,b], A. Pompili[a,b], G. Pugliese[a,c], A. Ranieri[a], G. Selvaggi[a,b], L. Silvestris[a], F.M. Simone[a,b], R. Venditti[a], P. Verwilligen[a]

**INFN Sezione di Bologna [a], Università di Bologna [b], Bologna, Italy**
G. Abbiendi[a], C. Battilana[a,b], D. Bonacorsi[a,b], L. Borgonovi[a], L. Brigliadori[a], R. Campanini[a,b], P. Capiluppi[a,b], A. Castro[a,b], F.R. Cavallo[a], M. Cuffiani[a,b], G.M. Dallavalle[a], T. Diotalevi[a,b], F. Fabbri[a], A. Fanfani[a,b], P. Giacomelli[a], L. Giommi[a,b], C. Grandi[a], L. Guiducci[a,b], S. Lo Meo[a,42], L. Lunerti[a,b], S. Marcellini[a], G. Masetti[a], F.L. Navarria[a,b], A. Perrotta[a], F. Primavera[a,b], A.M. Rossi[a,b], T. Rovelli[a,b], G.P. Siroli[a,b]

**INFN Sezione di Catania [a], Università di Catania [b], Catania, Italy**
S. Albergo[a,b,43], S. Costa[a,b,43], A. Di Mattia[a], R. Potenza[a,b], A. Tricomi[a,b,43], C. Tuve[a,b]

**INFN Sezione di Firenze [a], Università di Firenze [b], Firenze, Italy**
G. Barbagli[a], A. Cassese[a], R. Ceccarelli[a,b], V. Ciulli[a,b], C. Civinini[a], R. D'Alessandro[a,b], E. Focardi[a,b], G. Latino[a,b], P. Lenzi[a,b], M. Lizzo[a,b], M. Meschini[a], S. Paoletti[a], R. Seidita[a,b], G. Sguazzoni[a], L. Viliani[a]

**INFN Laboratori Nazionali di Frascati, Frascati, Italy**
L. Benussi, S. Bianco, D. Piccolo

**INFN Sezione di Genova [a], Università di Genova [b], Genova, Italy**
M. Bozzo[a,b], F. Ferro[a], R. Mulargia[a,b], E. Robutti[a], S. Tosi[a,b]

**INFN Sezione di Milano-Bicocca [a], Università di Milano-Bicocca [b], Milano, Italy**
A. Benaglia[a], F. Brivio[a,b], F. Cetorelli[a,b], V. Ciriolo[a,b,19], F. De Guio[a,b], M.E. Dinardo[a,b], P. Dini[a], S. Gennai[a], A. Ghezzi[a,b], P. Govoni[a,b], L. Guzzi[a,b], M. Malberti[a], S. Malvezzi[a], A. Massironi[a], D. Menasce[a], L. Moroni[a], M. Paganoni[a,b], D. Pedrini[a], S. Ragazzi[a,b], N. Redaelli[a], T. Tabarelli de Fatis[a,b], D. Valsecchi[a,b,19], D. Zuolo[a,b]

**INFN Sezione di Napoli [a], Università di Napoli 'Federico II' [b], Napoli, Italy, Università della Basilicata [c], Potenza, Italy, Università G. Marconi [d], Roma, Italy**
S. Buontempo[a], F. Carnevali[a,b], N. Cavallo[a,c], A. De Iorio[a,b], F. Fabozzi[a,c], A.O.M. Iorio[a,b], L. Lista[a,b], S. Meola[a,d,19], P. Paolucci[a,19], B. Rossi[a], C. Sciacca[a,b]

**INFN Sezione di Padova [a], Università di Padova [b], Padova, Italy, Università di Trento [c], Trento, Italy**
P. Azzi[a], N. Bacchetta[a], D. Bisello[a,b], P. Bortignon[a], A. Bragagnolo[a,b], R. Carlin[a,b], P. Checchia[a], T. Dorigo[a], U. Dosselli[a], F. Gasparini[a,b], U. Gasparini[a,b], S.Y. Hoh[a,b], L. Layer[a,44], M. Margoni[a,b], A.T. Meneguzzo[a,b], J. Pazzini[a,b], M. Presilla[a,b], P. Ronchese[a,b], R. Rossin[a,b], F. Simonetto[a,b], G. Strong[a], M. Tosi[a,b], H. YARAR[a,b], M. Zanetti[a,b], P. Zotto[a,b], A. Zucchetta[a,b], G. Zumerle[a,b]

**INFN Sezione di Pavia [a], Università di Pavia [b], Pavia, Italy**
C. Aime'[a,b], A. Braghieri[a], S. Calzaferri[a,b], D. Fiorina[a,b], P. Montagna[a,b], S.P. Ratti[a,b], V. Re[a], C. Riccardi[a,b], P. Salvini[a], I. Vai[a], P. Vitulo[a,b]

**INFN Sezione di Perugia [a], Università di Perugia [b], Perugia, Italy**
P. Asenov[a,45], G.M. Bilei[a], D. Ciangottini[a,b], L. Fanò[a,b], P. Lariccia[a,b], M. Magherini[b], G. Mantovani[a,b], V. Mariani[a,b], M. Menichelli[a], F. Moscatelli[a,45], A. Piccinelli[a,b], A. Rossi[a,b], A. Santocchia[a,b], D. Spiga[a], T. Tedeschi[a,b]

**INFN Sezione di Pisa [a], Università di Pisa [b], Scuola Normale Superiore di Pisa [c], Pisa Italy, Università di Siena [d], Siena, Italy**
P. Azzurri[a], G. Bagliesi[a], V. Bertacchi[a,c], L. Bianchini[a], T. Boccali[a], E. Bossini[a,b], R. Castaldi[a], M.A. Ciocci[a,b], V. D'Amante[a,d], R. Dell'Orso[a], M.R. Di Domenico[a,d], S. Donato[a], A. Giassi[a], F. Ligabue[a,c], E. Manca[a,c], G. Mandorli[a,c], A. Messineo[a,b], F. Palla[a], S. Parolia[a,b], G. Ramirez-Sanchez[a,c], A. Rizzi[a,b], G. Rolandi[a,c], S. Roy Chowdhury[a,c], A. Scribano[a], N. Shafiei[a,b], P. Spagnolo[a], R. Tenchini[a], G. Tonelli[a,b], N. Turini[a,d], A. Venturi[a], P.G. Verdini[a]

**INFN Sezione di Roma [a], Sapienza Università di Roma [b], Rome, Italy**
M. Campana[a,b], F. Cavallari[a], M. Cipriani[a,b], D. Del Re[a,b], E. Di Marco[a], M. Diemoz[a], E. Longo[a,b], P. Meridiani[a], G. Organtini[a,b], F. Pandolfi[a], R. Paramatti[a,b], C. Quaranta[a,b], S. Rahatlou[a,b], C. Rovelli[a], F. Santanastasio[a,b], L. Soffi[a], R. Tramontano[a,b]

**INFN Sezione di Torino [a], Università di Torino [b], Torino, Italy, Università del Piemonte Orientale [c], Novara, Italy**
N. Amapane[a,b], R. Arcidiacono[a,c], S. Argiro[a,b], M. Arneodo[a,c], N. Bartosik[a], R. Bellan[a,b], A. Bellora[a,b], J. Berenguer Antequera[a,b], C. Biino[a], N. Cartiglia[a], S. Cometti[a], M. Costa[a,b], R. Covarelli[a,b], N. Demaria[a], B. Kiani[a,b], F. Legger[a], C. Mariotti[a], S. Maselli[a], E. Migliore[a,b], E. Monteil[a,b], M. Monteno[a], M.M. Obertino[a,b], G. Ortona[a], L. Pacher[a,b], N. Pastrone[a], M. Pelliccioni[a], G.L. Pinna Angioni[a,b], M. Ruspa[a,c], K. Shchelina[a,b], F. Siviero[a,b], V. Sola[a], A. Solano[a,b], D. Soldi[a,b], A. Staiano[a], M. Tornago[a,b], D. Trocino[a,b], A. Vagnerini

**INFN Sezione di Trieste [a], Università di Trieste [b], Trieste, Italy**
S. Belforte[a], V. Candelise[a,b], M. Casarsa[a], F. Cossutti[a], A. Da Rold[a,b], G. Della Ricca[a,b], G. Sorrentino[a,b], F. Vazzoler[a,b]

**Kyungpook National University, Daegu, Korea**
S. Dogra, C. Huh, B. Kim, D.H. Kim, G.N. Kim, J. Kim, J. Lee, S.W. Lee, C.S. Moon, Y.D. Oh, S.I. Pak, B.C. Radburn-Smith, S. Sekmen, Y.C. Yang

**Chonnam National University, Institute for Universe and Elementary Particles, Kwangju, Korea**
H. Kim, D.H. Moon

**Hanyang University, Seoul, Korea**
B. Francois, T.J. Kim, J. Park

**Korea University, Seoul, Korea**
S. Cho, S. Choi, Y. Go, B. Hong, K. Lee, K.S. Lee, J. Lim, J. Park, S.K. Park, J. Yoo

**Kyung Hee University, Department of Physics, Seoul, Republic of Korea**
J. Goh, A. Gurtu

**Sejong University, Seoul, Korea**
H.S. Kim, Y. Kim

**Seoul National University, Seoul, Korea**
J. Almond, J.H. Bhyun, J. Choi, S. Jeon, J. Kim, J.S. Kim, S. Ko, H. Kwon, H. Lee, S. Lee, B.H. Oh, M. Oh, S.B. Oh, H. Seo, U.K. Yang, I. Yoon

**University of Seoul, Seoul, Korea**
W. Jang, D. Jeon, D.Y. Kang, Y. Kang, J.H. Kim, S. Kim, B. Ko, J.S.H. Lee, Y. Lee, I.C. Park, Y. Roh, M.S. Ryu, D. Song, I.J. Watson, S. Yang

**Yonsei University, Department of Physics, Seoul, Korea**
S. Ha, H.D. Yoo

**Sungkyunkwan University, Suwon, Korea**
M. Choi, Y. Jeong, H. Lee, Y. Lee, I. Yu

**College of Engineering and Technology, American University of the Middle East (AUM), Egaila, Kuwait**
T. Beyrouthy, Y. Maghrbi

**Riga Technical University, Riga, Latvia**
T. Torims, V. Veckalns[46]

**Vilnius University, Vilnius, Lithuania**
M. Ambrozas, A. Juodagalvis, A. Rinkevicius, G. Tamulaitis

**National Centre for Particle Physics, Universiti Malaya, Kuala Lumpur, Malaysia**
N. Bin Norjoharuddeen, W.A.T. Wan Abdullah, M.N. Yusli, Z. Zolkapli

**Universidad de Sonora (UNISON), Hermosillo, Mexico**
J.F. Benitez, A. Castaneda Hernandez, M. León Coello, J.A. Murillo Quijada, A. Sehrawat, L. Valencia Palomo

**Centro de Investigacion y de Estudios Avanzados del IPN, Mexico City, Mexico**
G. Ayala, H. Castilla-Valdez, E. De La Cruz-Burelo, I. Heredia-De La Cruz[47], R. Lopez-Fernandez, C.A. Mondragon Herrera, D.A. Perez Navarro, A. Sanchez-Hernandez

**Universidad Iberoamericana, Mexico City, Mexico**
S. Carrillo Moreno, C. Oropeza Barrera, M. Ramirez-Garcia, F. Vazquez Valencia

**Benemerita Universidad Autonoma de Puebla, Puebla, Mexico**
I. Pedraza, H.A. Salazar Ibarguen, C. Uribe Estrada

**University of Montenegro, Podgorica, Montenegro**
J. Mijuskovic[48], N. Raicevic

**University of Auckland, Auckland, New Zealand**
D. Krofcheck

**University of Canterbury, Christchurch, New Zealand**
S. Bheesette, P.H. Butler

**National Centre for Physics, Quaid-I-Azam University, Islamabad, Pakistan**
A. Ahmad, M.I. Asghar, A. Awais, M.I.M. Awan, H.R. Hoorani, W.A. Khan, M.A. Shah, M. Shoaib, M. Waqas

**AGH University of Science and Technology Faculty of Computer Science, Electronics and Telecommunications, Krakow, Poland**
V. Avati, L. Grzanka, M. Malawski

**National Centre for Nuclear Research, Swierk, Poland**
H. Bialkowska, M. Bluj, B. Boimska, M. Górski, M. Kazana, M. Szleper, P. Zalewski

**Institute of Experimental Physics, Faculty of Physics, University of Warsaw, Warsaw, Poland**
K. Bunkowski, K. Doroba, A. Kalinowski, M. Konecki, J. Krolikowski, M. Walczak

**Laboratório de Instrumentação e Física Experimental de Partículas, Lisboa, Portugal**
M. Araujo, P. Bargassa, D. Bastos, A. Boletti, P. Faccioli, M. Gallinaro, J. Hollar, N. Leonardo, T. Niknejad, M. Pisano, J. Seixas, O. Toldaiev, J. Varela

**Joint Institute for Nuclear Research, Dubna, Russia**
S. Afanasiev, D. Budkouski, I. Golutvin, I. Gorbunov, V. Karjavine, V. Korenkov, A. Lanev, A. Malakhov, V. Matveev[49,50], V. Palichik, V. Perelygin, M. Savina, D. Seitova, V. Shalaev, S. Shmatov, S. Shulha, V. Smirnov, O. Teryaev, N. Voytishin, B.S. Yuldashev[51], A. Zarubin, I. Zhizhin

**Petersburg Nuclear Physics Institute, Gatchina (St. Petersburg), Russia**
G. Gavrilov, V. Golovtcov, Y. Ivanov, V. Kim[52], E. Kuznetsova[53], V. Murzin, V. Oreshkin, I. Smirnov, D. Sosnov, V. Sulimov, L. Uvarov, S. Volkov, A. Vorobyev

**Institute for Nuclear Research, Moscow, Russia**
Yu. Andreev, A. Dermenev, S. Gninenko, N. Golubev, A. Karneyeu, D. Kirpichnikov, M. Kirsanov, N. Krasnikov, A. Pashenkov, G. Pivovarov, D. Tlisov†, A. Toropin

**Institute for Theoretical and Experimental Physics named by A.I. Alikhanov of NRC 'Kurchatov Institute', Moscow, Russia**
V. Epshteyn, V. Gavrilov, N. Lychkovskaya, A. Nikitenko[54], V. Popov, A. Spiridonov, A. Stepennov, M. Toms, E. Vlasov, A. Zhokin

**Moscow Institute of Physics and Technology, Moscow, Russia**
T. Aushev

**National Research Nuclear University 'Moscow Engineering Physics Institute' (MEPhI), Moscow, Russia**
O. Bychkova, R. Chistov[55], M. Danilov[56], P. Parygin, S. Polikarpov[55]

**P.N. Lebedev Physical Institute, Moscow, Russia**
V. Andreev, M. Azarkin, I. Dremin, M. Kirakosyan, A. Terkulov

**Skobeltsyn Institute of Nuclear Physics, Lomonosov Moscow State University, Moscow, Russia**
A. Belyaev, E. Boos, V. Bunichev, M. Dubinin[57], L. Dudko, A. Gribushin, V. Klyukhin, N. Korneeva, I. Lokhtin, S. Obraztsov, M. Perfilov, V. Savrin, P. Volkov

**Novosibirsk State University (NSU), Novosibirsk, Russia**
V. Blinov[58], T. Dimova[58], L. Kardapoltsev[58], A. Kozyrev[58], I. Ovtin[58], Y. Skovpen[58]

**Institute for High Energy Physics of National Research Centre 'Kurchatov Institute', Protvino, Russia**
I. Azhgirey, I. Bayshev, D. Elumakhov, V. Kachanov, D. Konstantinov, P. Mandrik, V. Petrov, R. Ryutin, S. Slabospitskii, A. Sobol, S. Troshin, N. Tyurin, A. Uzunian, A. Volkov

**National Research Tomsk Polytechnic University, Tomsk, Russia**
A. Babaev, V. Okhotnikov

**Tomsk State University, Tomsk, Russia**
V. Borshch, V. Ivanchenko, E. Tcherniaev

**University of Belgrade: Faculty of Physics and VINCA Institute of Nuclear Sciences, Belgrade, Serbia**
P. Adzic[59], M. Dordevic, P. Milenovic, J. Milosevic

**Centro de Investigaciones Energéticas Medioambientales y Tecnológicas (CIEMAT), Madrid, Spain**
M. Aguilar-Benitez, J. Alcaraz Maestre, A. Álvarez Fernández, I. Bachiller, M. Barrio Luna, Cristina F. Bedoya, C.A. Carrillo Montoya, M. Cepeda, M. Cerrada, N. Colino, B. De La Cruz, A. Delgado Peris, J.P. Fernández Ramos, J. Flix, M.C. Fouz, O. Gonzalez Lopez, S. Goy Lopez, J.M. Hernandez, M.I. Josa, J. León Holgado, D. Moran, Á. Navarro Tobar, A. Pérez-Calero Yzquierdo, J. Puerta Pelayo, I. Redondo, L. Romero, S. Sánchez Navas, L. Urda Gómez, C. Willmott

**Universidad Autónoma de Madrid, Madrid, Spain**
J.F. de Trocóniz, R. Reyes-Almanza

**Universidad de Oviedo, Instituto Universitario de Ciencias y Tecnologías Espaciales de Asturias (ICTEA), Oviedo, Spain**
B. Alvarez Gonzalez, J. Cuevas, C. Erice, J. Fernandez Menendez, S. Folgueras, I. Gonzalez Caballero, J.R. González Fernández, E. Palencia Cortezon, C. Ramón Álvarez, J. Ripoll Sau, V. Rodríguez Bouza, A. Trapote, N. Trevisani

**Instituto de Física de Cantabria (IFCA), CSIC-Universidad de Cantabria, Santander, Spain**
J.A. Brochero Cifuentes, I.J. Cabrillo, A. Calderon, J. Duarte Campderros, M. Fernandez, C. Fernandez Madrazo, P.J. Fernández Manteca, A. García Alonso, G. Gomez, C. Martinez Rivero, P. Martinez Ruiz del Arbol, F. Matorras, P. Matorras Cuevas, J. Piedra Gomez, C. Prieels, T. Rodrigo, A. Ruiz-Jimeno, L. Scodellaro, I. Vila, J.M. Vizan Garcia

**University of Colombo, Colombo, Sri Lanka**
MK Jayananda, B. Kailasapathy[60], D.U.J. Sonnadara, DDC Wickramarathna

**University of Ruhuna, Department of Physics, Matara, Sri Lanka**
W.G.D. Dharmaratna, K. Liyanage, N. Perera, N. Wickramage

**CERN, European Organization for Nuclear Research, Geneva, Switzerland**
T.K. Aarrestad, D. Abbaneo, J. Alimena, E. Auffray, G. Auzinger, J. Baechler, P. Baillon[†], D. Barney, J. Bendavid, M. Bianco, A. Bocci, T. Camporesi, M. Capeans Garrido, G. Cerminara, S.S. Chhibra, L. Cristella, D. d'Enterria, A. Dabrowski, N. Daci, A. David, A. De Roeck, M.M. Defranchis, M. Deile, M. Dobson, M. Dünser, N. Dupont, A. Elliott-Peisert, N. Emriskova, F. Fallavollita[61], D. Fasanella, S. Fiorendi, A. Florent, G. Franzoni, W. Funk, S. Giani, D. Gigi, K. Gill, F. Glege, L. Gouskos, M. Haranko, J. Hegeman, Y. Iiyama, V. Innocente, T. James, P. Janot, J. Kaspar, J. Kieseler, M. Komm, N. Kratochwil, C. Lange, S. Laurila, P. Lecoq, K. Long, C. Lourenço, L. Malgeri, S. Mallios, M. Mannelli, A.C. Marini, F. Meijers, S. Mersi, E. Meschi, F. Moortgat, M. Mulders, S. Orfanelli, L. Orsini, F. Pantaleo, L. Pape, E. Perez, M. Peruzzi, A. Petrilli, G. Petrucciani, A. Pfeiffer, M. Pierini, D. Piparo, M. Pitt, H. Qu, T. Quast, D. Rabady, A. Racz, G. Reales Gutiérrez, M. Rieger, M. Rovere, H. Sakulin, J. Salfeld-Nebgen, S. Scarfi, C. Schäfer, C. Schwick, M. Selvaggi, A. Sharma, P. Silva, W. Snoeys, P. Sphicas[62], S. Summers, V.R. Tavolaro, D. Treille, A. Tsirou, G.P. Van Onsem, M. Verzetti, J. Wanczyk[63], K.A. Wozniak, W.D. Zeuner

**Paul Scherrer Institut, Villigen, Switzerland**
L. Caminada[64], A. Ebrahimi, W. Erdmann, R. Horisberger, Q. Ingram, H.C. Kaestli, D. Kotlinski, U. Langenegger, M. Missiroli, T. Rohe

**ETH Zurich - Institute for Particle Physics and Astrophysics (IPA), Zurich, Switzerland**
K. Androsov[63], M. Backhaus, P. Berger, A. Calandri, N. Chernyavskaya, A. De Cosa, G. Dissertori, M. Dittmar, M. Donegà, C. Dorfer, F. Eble, K. Gedia, F. Glessgen, T.A. Gómez Espinosa, C. Grab, D. Hits, W. Lustermann, A.-M. Lyon, R.A. Manzoni, C. Martin Perez, M.T. Meinhard, F. Nessi-Tedaldi, J. Niedziela, F. Pauss, V. Perovic, S. Pigazzini, M.G. Ratti, M. Reichmann, C. Reissel, T. Reitenspiess, B. Ristic, D. Ruini, D.A. Sanz Becerra, M. Schönenberger, V. Stampf, J. Steggemann[63], R. Wallny, D.H. Zhu

**Universität Zürich, Zurich, Switzerland**
C. Amsler[65], P. Bärtschi, C. Botta, D. Brzhechko, M.F. Canelli, K. Cormier, A. De Wit, R. Del Burgo, J.K. Heikkilä, M. Huwiler, A. Jofrehei, B. Kilminster, S. Leontsinis, A. Macchiolo, P. Meiring, V.M. Mikuni, U. Molinatti, I. Neutelings, A. Reimers, P. Robmann, S. Sanchez Cruz, K. Schweiger, Y. Takahashi

**National Central University, Chung-Li, Taiwan**
C. Adloff[66], C.M. Kuo, W. Lin, A. Roy, T. Sarkar[36], S.S. Yu

**National Taiwan University (NTU), Taipei, Taiwan**
L. Ceard, Y. Chao, K.F. Chen, P.H. Chen, W.-S. Hou, Y.y. Li, R.-S. Lu, E. Paganis, A. Psallidas, A. Steen, H.y. Wu, E. Yazgan, P.r. Yu

**Chulalongkorn University, Faculty of Science, Department of Physics, Bangkok, Thailand**
B. Asavapibhop, C. Asawatangtrakuldee, N. Srimanobhas

**Çukurova University, Physics Department, Science and Art Faculty, Adana, Turkey**
F. Boran, S. Damarseckin[67], Z.S. Demiroglu, F. Dolek, I. Dumanoglu[68], E. Eskut, Y. Guler, E. Gurpinar Guler[69], I. Hos[70], C. Isik, O. Kara, A. Kayis Topaksu, U. Kiminsu, G. Onengut, K. Ozdemir[71], A. Polatoz, A.E. Simsek, B. Tali[72], U.G. Tok, S. Turkcapar, I.S. Zorbakir, C. Zorbilmez

**Middle East Technical University, Physics Department, Ankara, Turkey**
B. Isildak[73], G. Karapinar[74], K. Ocalan[75], M. Yalvac[76]

**Bogazici University, Istanbul, Turkey**
B. Akgun, I.O. Atakisi, E. Gülmez, M. Kaya[77], O. Kaya[78], Ö. Özçelik, S. Tekten[79], E.A. Yetkin[80]

**Istanbul Technical University, Istanbul, Turkey**
A. Cakir, K. Cankocak[68], Y. Komurcu, S. Sen[81]

**Istanbul University, Istanbul, Turkey**
S. Cerci[72], B. Kaynak, S. Ozkorucuklu, D. Sunar Cerci[72]

**Institute for Scintillation Materials of National Academy of Science of Ukraine, Kharkov, Ukraine**
B. Grynyov

**National Scientific Center, Kharkov Institute of Physics and Technology, Kharkov, Ukraine**
L. Levchuk

**University of Bristol, Bristol, United Kingdom**
D. Anthony, E. Bhal, S. Bologna, J.J. Brooke, A. Bundock, E. Clement, D. Cussans, H. Flacher, J. Goldstein, G.P. Heath, H.F. Heath, M.l. Holmberg[82], L. Kreczko, B. Krikler, S. Paramesvaran, S. Seif El Nasr-Storey, V.J. Smith, N. Stylianou[83], K. Walkingshaw Pass, R. White

**Rutherford Appleton Laboratory, Didcot, United Kingdom**
K.W. Bell, A. Belyaev[84], C. Brew, R.M. Brown, D.J.A. Cockerill, C. Cooke, K.V. Ellis, K. Harder,

S. Harper, J. Linacre, K. Manolopoulos, D.M. Newbold, E. Olaiya, D. Petyt, T. Reis, T. Schuh, C.H. Shepherd-Themistocleous, I.R. Tomalin, T. Williams

**Imperial College, London, United Kingdom**
R. Bainbridge, P. Bloch, S. Bonomally, J. Borg, S. Breeze, O. Buchmuller, V. Cepaitis, G.S. Chahal[85], D. Colling, P. Dauncey, G. Davies, M. Della Negra, S. Fayer, G. Fedi, G. Hall, M.H. Hassanshahi, G. Iles, J. Langford, L. Lyons, A.-M. Magnan, S. Malik, A. Martelli, D.G. Monk, J. Nash[86], M. Pesaresi, D.M. Raymond, A. Richards, A. Rose, E. Scott, C. Seez, A. Shtipliyski, A. Tapper, K. Uchida, T. Virdee[19], M. Vojinovic, N. Wardle, S.N. Webb, D. Winterbottom, A.G. Zecchinelli

**Brunel University, Uxbridge, United Kingdom**
K. Coldham, J.E. Cole, A. Khan, P. Kyberd, I.D. Reid, L. Teodorescu, S. Zahid

**Baylor University, Waco, USA**
S. Abdullin, A. Brinkerhoff, B. Caraway, J. Dittmann, K. Hatakeyama, A.R. Kanuganti, B. McMaster, N. Pastika, M. Saunders, S. Sawant, C. Sutantawibul, J. Wilson

**Catholic University of America, Washington, DC, USA**
R. Bartek, A. Dominguez, R. Uniyal, A.M. Vargas Hernandez

**The University of Alabama, Tuscaloosa, USA**
A. Buccilli, S.I. Cooper, D. Di Croce, S.V. Gleyzer, C. Henderson, C.U. Perez, P. Rumerio[87], C. West

**Boston University, Boston, USA**
A. Akpinar, A. Albert, D. Arcaro, C. Cosby, Z. Demiragli, E. Fontanesi, D. Gastler, J. Rohlf, K. Salyer, D. Sperka, D. Spitzbart, I. Suarez, A. Tsatsos, S. Yuan, D. Zou

**Brown University, Providence, USA**
G. Benelli, B. Burkle, X. Coubez[20], D. Cutts, M. Hadley, U. Heintz, J.M. Hogan[88], G. Landsberg, K.T. Lau, M. Lukasik, J. Luo, M. Narain, S. Sagir[89], E. Usai, W.Y. Wong, X. Yan, D. Yu, W. Zhang

**University of California, Davis, Davis, USA**
J. Bonilla, C. Brainerd, R. Breedon, M. Calderon De La Barca Sanchez, M. Chertok, J. Conway, P.T. Cox, R. Erbacher, G. Haza, F. Jensen, O. Kukral, R. Lander, M. Mulhearn, D. Pellett, B. Regnery, D. Taylor, Y. Yao, F. Zhang

**University of California, Los Angeles, USA**
M. Bachtis, R. Cousins, A. Datta, D. Hamilton, J. Hauser, M. Ignatenko, M.A. Iqbal, T. Lam, W.A. Nash, S. Regnard, D. Saltzberg, B. Stone, V. Valuev

**University of California, Riverside, Riverside, USA**
K. Burt, Y. Chen, R. Clare, J.W. Gary, M. Gordon, G. Hanson, G. Karapostoli, O.R. Long, N. Manganelli, M. Olmedo Negrete, W. Si, S. Wimpenny, Y. Zhang

**University of California, San Diego, La Jolla, USA**
J.G. Branson, P. Chang, S. Cittolin, S. Cooperstein, N. Deelen, D. Diaz, J. Duarte, R. Gerosa, L. Giannini, D. Gilbert, J. Guiang, R. Kansal, V. Krutelyov, R. Lee, J. Letts, M. Masciovecchio, S. May, M. Pieri, B.V. Sathia Narayanan, V. Sharma, M. Tadel, A. Vartak, F. Würthwein, Y. Xiang, A. Yagil

**University of California, Santa Barbara - Department of Physics, Santa Barbara, USA**
N. Amin, C. Campagnari, M. Citron, A. Dorsett, V. Dutta, J. Incandela, M. Kilpatrick, J. Kim, B. Marsh, H. Mei, M. Oshiro, M. Quinnan, J. Richman, U. Sarica, J. Sheplock, D. Stuart, S. Wang

**California Institute of Technology, Pasadena, USA**
A. Bornheim, O. Cerri, I. Dutta, J.M. Lawhorn, N. Lu, J. Mao, H.B. Newman, J. Ngadiuba, T.Q. Nguyen, M. Spiropulu, J.R. Vlimant, C. Wang, S. Xie, Z. Zhang, R.Y. Zhu

**Carnegie Mellon University, Pittsburgh, USA**
J. Alison, S. An, M.B. Andrews, P. Bryant, T. Ferguson, A. Harilal, C. Liu, T. Mudholkar, M. Paulini, A. Sanchez

**University of Colorado Boulder, Boulder, USA**
J.P. Cumalat, W.T. Ford, A. Hassani, E. MacDonald, R. Patel, A. Perloff, C. Savard, K. Stenson, K.A. Ulmer, S.R. Wagner

**Cornell University, Ithaca, USA**
J. Alexander, S. Bright-thonney, Y. Cheng, D.J. Cranshaw, S. Hogan, J. Monroy, J.R. Patterson, D. Quach, J. Reichert, M. Reid, A. Ryd, W. Sun, J. Thom, P. Wittich, R. Zou

**Fermi National Accelerator Laboratory, Batavia, USA**
M. Albrow, M. Alyari, G. Apollinari, A. Apresyan, A. Apyan, S. Banerjee, L.A.T. Bauerdick, D. Berry, J. Berryhill, P.C. Bhat, K. Burkett, J.N. Butler, A. Canepa, G.B. Cerati, H.W.K. Cheung, F. Chlebana, M. Cremonesi, K.F. Di Petrillo, V.D. Elvira, Y. Feng, J. Freeman, Z. Gecse, L. Gray, D. Green, S. Grünendahl, O. Gutsche, R.M. Harris, R. Heller, T.C. Herwig, J. Hirschauer, B. Jayatilaka, S. Jindariani, M. Johnson, U. Joshi, T. Klijnsma, B. Klima, K.H.M. Kwok, S. Lammel, D. Lincoln, R. Lipton, T. Liu, C. Madrid, K. Maeshima, C. Mantilla, D. Mason, P. McBride, P. Merkel, S. Mrenna, S. Nahn, V. O'Dell, V. Papadimitriou, K. Pedro, C. Pena[57], O. Prokofyev, F. Ravera, A. Reinsvold Hall, L. Ristori, B. Schneider, E. Sexton-Kennedy, N. Smith, A. Soha, W.J. Spalding, L. Spiegel, S. Stoynev, J. Strait, L. Taylor, S. Tkaczyk, N.V. Tran, L. Uplegger, E.W. Vaandering, H.A. Weber

**University of Florida, Gainesville, USA**
D. Acosta, P. Avery, D. Bourilkov, L. Cadamuro, V. Cherepanov, F. Errico, R.D. Field, D. Guerrero, B.M. Joshi, M. Kim, E. Koenig, J. Konigsberg, A. Korytov, K.H. Lo, K. Matchev, N. Menendez, G. Mitselmakher, A. Muthirakalayil Madhu, N. Rawal, D. Rosenzweig, S. Rosenzweig, K. Shi, J. Sturdy, J. Wang, E. Yigitbasi, X. Zuo

**Florida State University, Tallahassee, USA**
T. Adams, A. Askew, R. Habibullah, V. Hagopian, K.F. Johnson, R. Khurana, T. Kolberg, G. Martinez, H. Prosper, C. Schiber, O. Viazlo, R. Yohay, J. Zhang

**Florida Institute of Technology, Melbourne, USA**
M.M. Baarmand, S. Butalla, T. Elkafrawy[90], M. Hohlmann, R. Kumar Verma, D. Noonan, M. Rahmani, F. Yumiceva

**University of Illinois at Chicago (UIC), Chicago, USA**
M.R. Adams, H. Becerril Gonzalez, R. Cavanaugh, X. Chen, S. Dittmer, O. Evdokimov, C.E. Gerber, D.A. Hangal, D.J. Hofman, A.H. Merrit, C. Mills, G. Oh, T. Roy, S. Rudrabhatla, M.B. Tonjes, N. Varelas, J. Viinikainen, X. Wang, Z. Wu, Z. Ye

**The University of Iowa, Iowa City, USA**
M. Alhusseini, K. Dilsiz[91], R.P. Gandrajula, O.K. Köseyan, J.-P. Merlo, A. Mestvirishvili[92], J. Nachtman, H. Ogul[93], Y. Onel, A. Penzo, C. Snyder, E. Tiras[94]

**Johns Hopkins University, Baltimore, USA**
O. Amram, B. Blumenfeld, L. Corcodilos, J. Davis, M. Eminizer, A.V. Gritsan, S. Kyriacou, P. Maksimovic, J. Roskes, M. Swartz, T.Á. Vámi

**The University of Kansas, Lawrence, USA**
A. Abreu, J. Anguiano, C. Baldenegro Barrera, P. Baringer, A. Bean, A. Bylinkin, Z. Flowers, T. Isidori, S. Khalil, J. King, G. Krintiras, A. Kropivnitskaya, M. Lazarovits, C. Lindsey, J. Marquez, N. Minafra, M. Murray, M. Nickel, C. Rogan, C. Royon, R. Salvatico, S. Sanders, E. Schmitz, C. Smith, J.D. Tapia Takaki, Q. Wang, Z. Warner, J. Williams, G. Wilson

**Kansas State University, Manhattan, USA**
S. Duric, A. Ivanov, K. Kaadze, D. Kim, Y. Maravin, T. Mitchell, A. Modak, K. Nam

**Lawrence Livermore National Laboratory, Livermore, USA**
F. Rebassoo, D. Wright

**University of Maryland, College Park, USA**
E. Adams, A. Baden, O. Baron, A. Belloni, S.C. Eno, N.J. Hadley, S. Jabeen, R.G. Kellogg, T. Koeth, A.C. Mignerey, S. Nabili, M. Seidel, A. Skuja, L. Wang, K. Wong

**Massachusetts Institute of Technology, Cambridge, USA**
D. Abercrombie, G. Andreassi, R. Bi, S. Brandt, W. Busza, I.A. Cali, Y. Chen, M. D'Alfonso, J. Eysermans, C. Freer, G. Gomez Ceballos, M. Goncharov, P. Harris, M. Hu, M. Klute, D. Kovalskyi, J. Krupa, Y.-J. Lee, B. Maier, C. Mironov, C. Paus, D. Rankin, C. Roland, G. Roland, Z. Shi, G.S.F. Stephans, K. Tatar, J. Wang, Z. Wang, B. Wyslouch

**University of Minnesota, Minneapolis, USA**
R.M. Chatterjee, A. Evans, P. Hansen, J. Hiltbrand, Sh. Jain, M. Krohn, Y. Kubota, J. Mans, M. Revering, R. Rusack, R. Saradhy, N. Schroeder, N. Strobbe, M.A. Wadud

**University of Nebraska-Lincoln, Lincoln, USA**
K. Bloom, M. Bryson, S. Chauhan, D.R. Claes, C. Fangmeier, L. Finco, F. Golf, C. Joo, I. Kravchenko, M. Musich, I. Reed, J.E. Siado, G.R. Snow[†], W. Tabb, F. Yan

**State University of New York at Buffalo, Buffalo, USA**
G. Agarwal, H. Bandyopadhyay, L. Hay, I. Iashvili, A. Kharchilava, C. McLean, D. Nguyen, J. Pekkanen, S. Rappoccio, A. Williams

**Northeastern University, Boston, USA**
G. Alverson, E. Barberis, Y. Haddad, A. Hortiangtham, J. Li, G. Madigan, B. Marzocchi, D.M. Morse, V. Nguyen, T. Orimoto, A. Parker, L. Skinnari, A. Tishelman-Charny, T. Wamorkar, B. Wang, A. Wisecarver, D. Wood

**Northwestern University, Evanston, USA**
S. Bhattacharya, J. Bueghly, Z. Chen, A. Gilbert, T. Gunter, K.A. Hahn, Y. Liu, N. Odell, M.H. Schmitt, M. Velasco

**University of Notre Dame, Notre Dame, USA**
R. Band, R. Bucci, A. Das, N. Dev, R. Goldouzian, M. Hildreth, K. Hurtado Anampa, C. Jessop, K. Lannon, J. Lawrence, N. Loukas, D. Lutton, N. Marinelli, I. Mcalister, T. McCauley, F. Meng, K. Mohrman, Y. Musienko[49], R. Ruchti, P. Siddireddy, A. Townsend, M. Wayne, A. Wightman, M. Wolf, M. Zarucki, L. Zygala

**The Ohio State University, Columbus, USA**
B. Bylsma, B. Cardwell, L.S. Durkin, B. Francis, C. Hill, M. Nunez Ornelas, K. Wei, B.L. Winer, B.R. Yates

**Princeton University, Princeton, USA**
F.M. Addesa, B. Bonham, P. Das, G. Dezoort, P. Elmer, A. Frankenthal, B. Greenberg,

N. Haubrich, S. Higginbotham, A. Kalogeropoulos, G. Kopp, S. Kwan, D. Lange, M.T. Lucchini, D. Marlow, K. Mei, I. Ojalvo, J. Olsen, C. Palmer, D. Stickland, C. Tully

**University of Puerto Rico, Mayaguez, USA**
S. Malik, S. Norberg

**Purdue University, West Lafayette, USA**
A.S. Bakshi, V.E. Barnes, R. Chawla, S. Das, L. Gutay, M. Jones, A.W. Jung, S. Karmarkar, M. Liu, G. Negro, N. Neumeister, G. Paspalaki, C.C. Peng, S. Piperov, A. Purohit, J.F. Schulte, M. Stojanovic[15], J. Thieman, F. Wang, R. Xiao, W. Xie

**Purdue University Northwest, Hammond, USA**
J. Dolen, N. Parashar

**Rice University, Houston, USA**
A. Baty, M. Decaro, S. Dildick, K.M. Ecklund, S. Freed, P. Gardner, F.J.M. Geurts, A. Kumar, W. Li, B.P. Padley, R. Redjimi, W. Shi, A.G. Stahl Leiton, S. Yang, L. Zhang, Y. Zhang

**University of Rochester, Rochester, USA**
A. Bodek, P. de Barbaro, R. Demina, J.L. Dulemba, C. Fallon, T. Ferbel, M. Galanti, A. Garcia-Bellido, O. Hindrichs, A. Khukhunaishvili, E. Ranken, R. Taus

**Rutgers, The State University of New Jersey, Piscataway, USA**
B. Chiarito, J.P. Chou, A. Gandrakota, Y. Gershtein, E. Halkiadakis, A. Hart, M. Heindl, O. Karacheban[23], I. Laflotte, A. Lath, R. Montalvo, K. Nash, M. Osherson, S. Salur, S. Schnetzer, S. Somalwar, R. Stone, S.A. Thayil, S. Thomas, H. Wang

**University of Tennessee, Knoxville, USA**
H. Acharya, A.G. Delannoy, S. Spanier

**Texas A&M University, College Station, USA**
O. Bouhali[95], M. Dalchenko, A. Delgado, R. Eusebi, J. Gilmore, T. Huang, T. Kamon[96], H. Kim, S. Luo, S. Malhotra, R. Mueller, D. Overton, D. Rathjens, A. Safonov

**Texas Tech University, Lubbock, USA**
N. Akchurin, J. Damgov, V. Hegde, S. Kunori, K. Lamichhane, S.W. Lee, T. Mengke, S. Muthumuni, T. Peltola, I. Volobouev, Z. Wang, A. Whitbeck

**Vanderbilt University, Nashville, USA**
E. Appelt, S. Greene, A. Gurrola, W. Johns, A. Melo, H. Ni, K. Padeken, F. Romeo, P. Sheldon, S. Tuo, J. Velkovska

**University of Virginia, Charlottesville, USA**
M.W. Arenton, B. Cox, G. Cummings, J. Hakala, R. Hirosky, M. Joyce, A. Ledovskoy, A. Li, C. Neu, B. Tannenwald, S. White, E. Wolfe

**Wayne State University, Detroit, USA**
R. Harr, N. Poudyal

**University of Wisconsin - Madison, Madison, WI, USA**
K. Black, T. Bose, J. Buchanan, C. Caillol, S. Dasu, I. De Bruyn, P. Everaerts, F. Fienga, C. Galloni, H. He, M. Herndon, A. Hervé, U. Hussain, A. Lanaro, A. Loeliger, R. Loveless, J. Madhusudanan Sreekala, A. Mallampalli, A. Mohammadi, D. Pinna, A. Savin, V. Shang, V. Sharma, W.H. Smith, D. Teague, S. Trembath-reichert, W. Vetens

†: Deceased
1: Also at TU Wien, Wien, Austria
2: Also at Institute of Basic and Applied Sciences, Faculty of Engineering, Arab Academy for Science, Technology and Maritime Transport, Alexandria, Egypt, Alexandria, Egypt
3: Also at Université Libre de Bruxelles, Bruxelles, Belgium
4: Also at Universidade Estadual de Campinas, Campinas, Brazil
5: Also at Federal University of Rio Grande do Sul, Porto Alegre, Brazil
6: Also at University of Chinese Academy of Sciences, Beijing, China
7: Also at Department of Physics, Tsinghua University, Beijing, China, Beijing, China
8: Also at UFMS, Nova Andradina, Brazil
9: Also at Nanjing Normal University Department of Physics, Nanjing, China
10: Now at The University of Iowa, Iowa City, USA
11: Also at Institute for Theoretical and Experimental Physics named by A.I. Alikhanov of NRC 'Kurchatov Institute', Moscow, Russia
12: Also at Joint Institute for Nuclear Research, Dubna, Russia
13: Also at Cairo University, Cairo, Egypt
14: Also at Zewail City of Science and Technology, Zewail, Egypt
15: Also at Purdue University, West Lafayette, USA
16: Also at Université de Haute Alsace, Mulhouse, France
17: Also at Tbilisi State University, Tbilisi, Georgia
18: Also at Erzincan Binali Yildirim University, Erzincan, Turkey
19: Also at CERN, European Organization for Nuclear Research, Geneva, Switzerland
20: Also at RWTH Aachen University, III. Physikalisches Institut A, Aachen, Germany
21: Also at University of Hamburg, Hamburg, Germany
22: Also at Department of Physics, Isfahan University of Technology, Isfahan, Iran, Isfahan, Iran
23: Also at Brandenburg University of Technology, Cottbus, Germany
24: Also at Skobeltsyn Institute of Nuclear Physics, Lomonosov Moscow State University, Moscow, Russia
25: Also at Physics Department, Faculty of Science, Assiut University, Assiut, Egypt
26: Also at Karoly Robert Campus, MATE Institute of Technology, Gyongyos, Hungary
27: Also at Institute of Physics, University of Debrecen, Debrecen, Hungary, Debrecen, Hungary
28: Also at Institute of Nuclear Research ATOMKI, Debrecen, Hungary
29: Also at MTA-ELTE Lendület CMS Particle and Nuclear Physics Group, Eötvös Loránd University, Budapest, Hungary, Budapest, Hungary
30: Also at Wigner Research Centre for Physics, Budapest, Hungary
31: Also at IIT Bhubaneswar, Bhubaneswar, India, Bhubaneswar, India
32: Also at Institute of Physics, Bhubaneswar, India
33: Also at G.H.G. Khalsa College, Punjab, India
34: Also at Shoolini University, Solan, India
35: Also at University of Hyderabad, Hyderabad, India
36: Also at University of Visva-Bharati, Santiniketan, India
37: Also at Indian Institute of Technology (IIT), Mumbai, India
38: Also at Deutsches Elektronen-Synchrotron, Hamburg, Germany
39: Also at Sharif University of Technology, Tehran, Iran
40: Also at Department of Physics, University of Science and Technology of Mazandaran, Behshahr, Iran
41: Now at INFN Sezione di Bari [a], Università di Bari [b], Politecnico di Bari [c], Bari, Italy

42: Also at Italian National Agency for New Technologies, Energy and Sustainable Economic Development, Bologna, Italy
43: Also at Centro Siciliano di Fisica Nucleare e di Struttura Della Materia, Catania, Italy
44: Also at Università di Napoli 'Federico II', NAPOLI, Italy
45: Also at Consiglio Nazionale delle Ricerche - Istituto Officina dei Materiali, PERUGIA, Italy
46: Also at Riga Technical University, Riga, Latvia, Riga, Latvia
47: Also at Consejo Nacional de Ciencia y Tecnología, Mexico City, Mexico
48: Also at IRFU, CEA, Université Paris-Saclay, Gif-sur-Yvette, France
49: Also at Institute for Nuclear Research, Moscow, Russia
50: Now at National Research Nuclear University 'Moscow Engineering Physics Institute' (MEPhI), Moscow, Russia
51: Also at Institute of Nuclear Physics of the Uzbekistan Academy of Sciences, Tashkent, Uzbekistan
52: Also at St. Petersburg State Polytechnical University, St. Petersburg, Russia
53: Also at University of Florida, Gainesville, USA
54: Also at Imperial College, London, United Kingdom
55: Also at P.N. Lebedev Physical Institute, Moscow, Russia
56: Also at Moscow Institute of Physics and Technology, Moscow, Russia, Moscow, Russia
57: Also at California Institute of Technology, Pasadena, USA
58: Also at Budker Institute of Nuclear Physics, Novosibirsk, Russia
59: Also at Faculty of Physics, University of Belgrade, Belgrade, Serbia
60: Also at Trincomalee Campus, Eastern University, Sri Lanka, Nilaveli, Sri Lanka
61: Also at INFN Sezione di Pavia [a], Università di Pavia [b], Pavia, Italy, Pavia, Italy
62: Also at National and Kapodistrian University of Athens, Athens, Greece
63: Also at Ecole Polytechnique Fédérale Lausanne, Lausanne, Switzerland
64: Also at Universität Zürich, Zurich, Switzerland
65: Also at Stefan Meyer Institute for Subatomic Physics, Vienna, Austria, Vienna, Austria
66: Also at Laboratoire d'Annecy-le-Vieux de Physique des Particules, IN2P3-CNRS, Annecy-le-Vieux, France
67: Also at Şırnak University, Sirnak, Turkey
68: Also at Near East University, Research Center of Experimental Health Science, Nicosia, Turkey
69: Also at Konya Technical University, Konya, Turkey
70: Also at Istanbul University - Cerrahpasa, Faculty of Engineering, Istanbul, Turkey
71: Also at Piri Reis University, Istanbul, Turkey
72: Also at Adiyaman University, Adiyaman, Turkey
73: Also at Ozyegin University, Istanbul, Turkey
74: Also at Izmir Institute of Technology, Izmir, Turkey
75: Also at Necmettin Erbakan University, Konya, Turkey
76: Also at Bozok Universitetesi Rektörlügü, Yozgat, Turkey, Yozgat, Turkey
77: Also at Marmara University, Istanbul, Turkey
78: Also at Milli Savunma University, Istanbul, Turkey
79: Also at Kafkas University, Kars, Turkey
80: Also at Istanbul Bilgi University, Istanbul, Turkey
81: Also at Hacettepe University, Ankara, Turkey
82: Also at Rutherford Appleton Laboratory, Didcot, United Kingdom
83: Also at Vrije Universiteit Brussel, Brussel, Belgium
84: Also at School of Physics and Astronomy, University of Southampton, Southampton, United Kingdom

85: Also at IPPP Durham University, Durham, United Kingdom
86: Also at Monash University, Faculty of Science, Clayton, Australia
87: Also at Università di Torino, TORINO, Italy
88: Also at Bethel University, St. Paul, Minneapolis, USA, St. Paul, USA
89: Also at Karamanoğlu Mehmetbey University, Karaman, Turkey
90: Also at Ain Shams University, Cairo, Egypt
91: Also at Bingol University, Bingol, Turkey
92: Also at Georgian Technical University, Tbilisi, Georgia
93: Also at Sinop University, Sinop, Turkey
94: Also at Erciyes University, KAYSERI, Turkey
95: Also at Texas A&M University at Qatar, Doha, Qatar
96: Also at Kyungpook National University, Daegu, Korea, Daegu, Korea